

San Albino, Nicaragua: A Low-Angle, Thrust-Controlled Orogenic Gold Deposit

Rael D. Lipson, ^{1,2,†} Richard J. Goldfarb, ^{3,4} Ben M. Frieman, ⁴ and John Payne ⁵

¹RDLGEO Consulting Inc., 12654 Plaza Menta, San Diego, California 92128, USA

²Mako Mining Corp., 838 West Hastings St., Suite 700, Vancouver, British Columbia V6C 0A6, Canada

³ State Key Laboratory of Geological Processes and Mineral Resources, China University of Geosciences, Beijing 100083, China

⁴Department of Geology and Geological Engineering, Colorado School of Mines, Golden, Colorado 80401, USA

⁵ Vancouver Petrographics Ltd., 8080 Glover Road, Langley, British Columbia V1M 3S3, Canada

Abstract

The San Albino deposit is an orogenic gold occurrence hosted by a low-angle thrust that is the site of a new open-pit mine in northern Nicaragua. The deposit is hosted in greenschist facies rocks of the Jurassic metasedimentary Neuvo Segovia Formation. The schist was uplifted and exposed during arc accretion and Cretaceous thin-skin deformation, forming the NE-striking Colon fold-and-thrust belt. Deformation included emplacement of the 119 to 113 Ma NE-trending Dipilto batholith into the regionally metamorphosed clastic rocks about 5 km northwest of the San Albino deposit. Mineralization is dominated by three laminated quartz vein systems (i.e., San Albino, Naranjo, Arras) that broadly follow shallowly dipping (approx. 30°) carbonaceous shears roughly concordant to schistosity along the limbs of a doubly plunging antiform. The three main parallel shears are each separated by about 90 m and individually reach a maximum thickness of about 8 m. Maximum thickness of ore zones is where post-ore local folding and reverse motion along the shallow shears has duplicated the laminated low-angle gold-bearing veins (D2 and early D3). Additional gold was added to the veins, with abundant sulfides, during a subsequent brecciation event of the early formed quartz veins that accompanied progressive thrusting (late D₃). This predated boudinage of the veins during continued compression and thrust loading (D4); high gold grades are particularly notable along pyrite- and arsenopyrite-bearing stylolites formed during D_4 pressure solution. The D_2 to D_3 gold event is likely coeval with Albian uplift of the Dipilto batholith and with back thrusting in the schist aided by the stress inhomogeneities provided by the igneous complex.

Low-angle thrust-controlled orogenic gold deposits may represent world-class exploration targets because of their large linear footprints, although they are traditionally looked at as less favorable exploration targets relative to gold systems developed more commonly along high-angle reverse faults. Our case study of the San Albino deposit shows that although low-angle deposits are not inherently misoriented for failure like the more common subvertical reverse fault-related deposits, they may be sites of significant pressure buildup due to hydrothermal mineral precipitation during initial water-rock interaction or slight temperature decreases along the low-angle flow path. Resulting fluid cycling may lead to thick laminated vein development, such as seen at San Albino, where especially high-grade zones may be associated with local steepening and/or dilational zones within the broader, low-angle vein-hosting shear system.

Introduction

Orogenic gold deposits form in a wide range of lithological and structural settings (Goldfarb et al., 2005), typically with mineralization extending over depths in excess of 1 km in complex arrays along steeply dipping structures. However, a subset of such deposits is relatively simple in form with a predominantly planar, shallowly dipping aspect. The San Albino gold deposit in Nicaragua, recently placed into production, is an example of such a low-angle, thrust-related orogenic gold deposit. Little academic work has been conducted to date on the deposit. This paper is the result of detailed geologic and structural mapping in the San Albino open-pit area prior to mining and at surrounding outcrops. In addition, it includes petrological and microstructural observations from drill core.

Orogenic deposits are typically not recognized as widespread gold targets in Central America, as explorationists have tended to focus their activity on historically important and past-producing epithermal precious metal systems (e.g., Rosario district, Guatemala; Carpenter, 1954). Nevertheless,

[†]Corresponding author: e-mail, rael.lipson@rdlgeo.com

and although with few detailed descriptions, gold systems probably best classified as orogenic are widespread in black shales and argillaceous phyllites and schists in Central America. These include those in the late Paleozoic metasedimentary clastic rocks of the Maya Mountains, such as in the Ceibo Chico area of Belize (Boiton Minerals Ltd, unpub. company report, 2018), at Tambor/El Sastre (Radius Gold, unpub. company report, 2004) and Ixtahuacan/Annabella (Guillemette and Williams-Jones, 1993) in Guatemala, and in the Canan area in the Lepaguare district of Honduras along the Guayape fault system to the north of San Albino (Mattioli et al., 2014). Thus, orogenic gold deposits represent a significant exploration target in Central America, despite poor delineation of their temporal and lithotectonic context within the region.

The study was initiated after similarities were recognized between the San Albino deposit in Nicaragua and the Macraes deposit in New Zealand (Lipson and Pudar, 2017), particularly in their low-angle thrust-related structural controls. These deposits represent a small group of such low-angle, thrust-related orogenic gold deposits and are less common and often overlooked relative to high-angle, thrust-related

orogenic gold deposits. Although from grade, size, and metallurgical perspectives San Albino and other low-angle deposits may show some significant differences, the structural setting and associated shear geometries are remarkably similar. Here, the San Albino deposit is described in detail, then compared to a diverse suite of low-angle, thrust-related deposits spanning a range of geologic environments and time periods from different parts of the world (Fig. 1A; Table 1). This study aims to establish a better conceptual framework for low-angle, thrust-related orogenic gold deposits, which have the potential to be prolific exploration targets. Furthermore, on a more applied and local level, it allows for a better understanding of ore controls that will enhance resource models.

Discovery and Exploration History of the San Albino Deposit

Quartz vein-hosted gold was discovered in 1790 in the San Albino area by the Spaniards, who later conducted a smallscale open-pit operation and then underground mining before the workings were flooded. Subsequent mining, mainly from 1885 through 1926, yielded an estimated 18,200 oz of gold with an average grade of 16 g/t (Roberts and Irving, 1957; J.M. Kowalchuk, unpub. report, 2011). The most successful of the operators during this period was an American, Charles Butters, who between 1922 and 1926 built a hydropowered mill and mined 3,000 short tons of ore. Mining from these operations ceased in 1926, when Augusto Sandino seized the mine and continued to mill stockpiled ore for a few years to finance the Sandinista revolution. Subsequently, only minor work was conducted by a series of operators on the property until 1981, when infrastructure was destroyed by revolutionaries. More recently, from 1996 to 1997, Western Mining Corporation conducted stream sediment, soil, and rock chip sampling programs, which included reopening and sampling of earlier-mined underground levels and drilled two vertical holes, which failed to reach the intended target depth of about 120 m. Pila Gold Ltd. explored for a large-tonnage, bulk mineable deposit in 2003, and Condor Resources Plc. drilled 25 holes between 2006 and 2009 that yielded high-grade gold intercepts including 4 m at 16.3 g/t Au.

Golden Reign Resources Ltd. acquired the property in 2009 and embarked on an extensive exploration campaign of rock chip and channel sampling of the numerous gold occurrences across the tenement. Regional and detailed mapping was followed by a program of auger soil sampling, which highlighted prospective zones, particularly in the Las Conchitas area, for follow-up trenching, sampling, and drilling. Soil and rock chip sampling showed that both lead and arsenic are good local pathfinders for gold, and scorodite-bearing quartz vein outcrops proved particularly helpful in locating the most prospective gold-bearing veins. In 2018, Golden Reign merged with Marlin Gold to form Mako Mining Corp., the current operator of mining and exploration activities at the San Albino deposit and surroundings.

At San Albino, between 2010 and 2020, 788 diamond drill holes and 191 reverse circulation holes were completed totaling 67,166 and 3,240 m, respectively. These drilling programs defined a measured plus indicated resource of 541,500 metric tonnes (t) for 178,000 oz Au at 10.2 g/t and 304,000 oz Ag at 17.4 g/t, plus an additional inferred resource of 421,600 t for

101,000 oz Au at 7.4 g/t and 170,000 oz Ag at 12.6 g/t. Commercial open-pit mining was initiated at San Albino in July 2021, based solely on resources and with a processing plant operating at a nominal rate of 500 tpd, which recovers gold by two-stage crushing, grinding, gravity concentration, and cyanide leaching using a standard carbon in leach (CIL) circuit. In addition, 310 diamond drill holes totaling 24,359 m were completed at Las Conchitas 2.5 km south of the San Albino mine from 2011 to 2020. Drilling is ongoing to establish a resource there (Ristorcelli et al., 2020) (Fig. 2B). Production in 2022, the first full year of operations, amounted to 199,967 t of ore, which when blended with historical stockpiles had a mill head grade of 7.36 g/t Au (and approx. 11 g/t Ag), making it one of the highest-grade open-pit gold mines in the world. Of the 47,292 oz of Au in ore milled, 37,678 oz were produced at a gold recovery of 79.8%. The mine strip ratio was unusually high at 27.1:1 waste to ore (Mako Mining, 2023b).

Regional Geologic Setting

The San Albino deposit, located in the Nueva Segovia Department of Nicaragua (Fig. 1B), is hosted within the Chortis block or Chortis superterrane (Rogers et al., 2007a), which is a composite microcontinent that forms much of Guatemala, El Salvador, Nicaragua, and Honduras. The superterrane has been subdivided into several poorly understood Mesoproterozoic-Mesozoic terranes (Rogers et al., 2007a; Ratschbacher et al., 2009) and is separated from the North American Plate to the north by the Motagua-Polochic transform fault system (Fig. 1B). Much of the superterrane may have at one time been part of northwestern South America or southwestern Mexico prior to being integrated into the Caribbean Plate (Garcia-Amador et al., 2021; Gazel et al., 2021). More recent tectonic models argue that the superterrane may consist of multiple basement blocks, each with distinct tectonothermal histories (Ortega-Gutiérrez et al., 2007; Rogers et al., 2007a; Garcia-Amador et al., 2021). Refinements to these models based on paleomagnetic reconstructions have recognized two distinct microblocks or terranes that are separated by the Guayape fault system (Fig. 1B), termed the Chortis and Dipilto terranes (Garcia-Amador et al., 2019). Stratigraphic correlations indicate that these two terranes may have been amalgamated into a single block as early as mid-Paleozoic (Gazel et al., 2021).

The San Albino deposit is hosted by clastic sedimentary rocks of the Neuva Segovia Formation of the Dipilto terrane. Sedimentary rocks in the Nueva Segovia Formation primarily consist of graphitic schists, with lesser metasandstone, and calc-silicate units, which locally are interlayered with felsic metavolcanic units (Garcia-Amador et al., 2021; Freeborne and Braid, 2023). In the western part of the terrane, these units are relatively unmetamorphosed, whereas throughout much of the terrane they show greenschist facies assemblages (Andjić et al., 2019). Burianek and Dolnicek. (2011), following Rogers et al. (2007a), noted that metasedimentary rocks in Nicaragua are a slightly more metamorphosed equivalent of the >1,700-m-thick Middle Jurassic weakly metamorphosed Agua Fria sandstones and shales in Honduras. Both Blandino et al. (2007) and Garcia-Amador et al. (2019) agree that this Mesozoic schist, alternatively termed the Neuva Segovia schist or Palacaguina Formation in Nicaragua, may be correlated

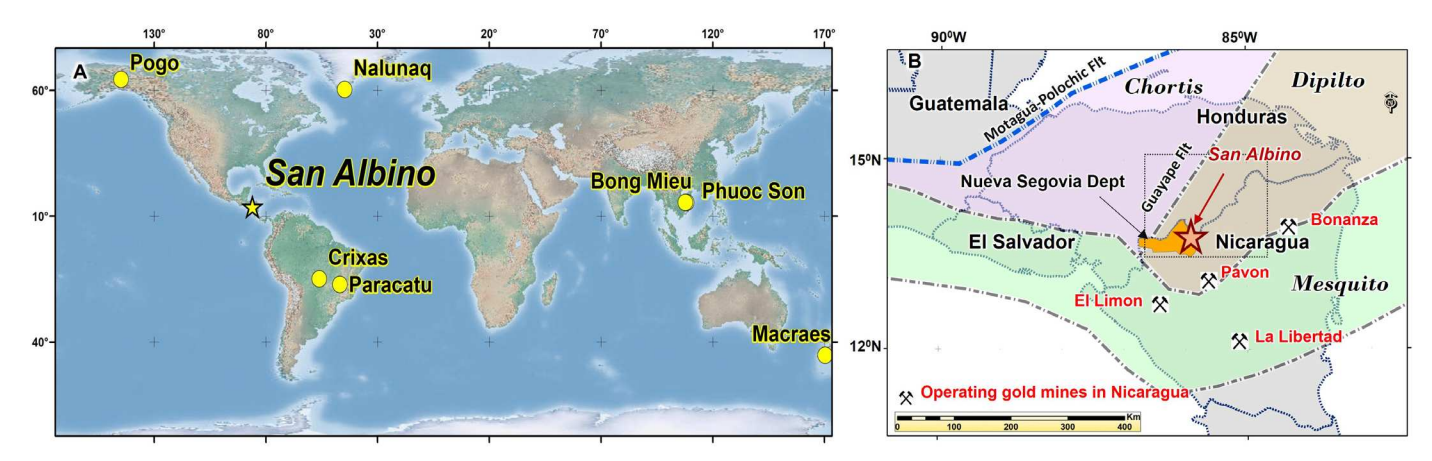


Fig. 1. A. Global occurrence of notable low-angle, thrust-related orogenic deposits. B. Map displaying the general boundaries for the Chortis, Dipilto, and Mesquito (or Siuna) terranes (or blocks) (after Garcia-Amador et al., 2021) along with the location of San Albino deposit in the Nueva Segovia Department (orange) of Nicaragua (modified from Andjić et al., 2019; Garcia-Amador et al., 2021). Note: dashed box indicates the location of Figure 2A. Flt = fault.

with the Agua Fria Formation, but this is not certain. These rocks are separated to the west from those of the Chortis terrane by the NE-striking Guayape fault system located about 15 to 20 km northwest of the Nicaragua border (Figs. 1B, 2A).

In Honduras, the Chortis terrane preserves Grenville-aged basement consisting of an older schist and gneiss as well as the Cacaguapa schist, which are both overlain by the Agua Fria Formation (Rogers, 2003; Andjić et al., 2019). The top of the Agua Fria Formation is marked by a major unconformity above which the Early Cretaceous Tepemichin red bed conglomerates were deposited and which are in turn overlain by the Atima Formation platform carbonates (Fig. 2A). However, in Nicaragua, no Proterozoic and Paleozoic basement rocks to the Neuvo Segovia schist are documented.

During mainly the Early to middle Cretaceous, the Jurassic-Early Cretaceous oceanic-arc rocks of the Mesquito (or Siuna) terrane were accreted along the southeastern margin of the Dipilto terrane (Andjić et al., 2019; Garcia-Amador et al., 2021). This resulted in widespread deformation and initial development of the Colon fold-and-thrust belt (Rogers et al., 2007b) in the Dipilto terrane (Figs. 1B, 2A). This major NE-striking fold-and-thrust belt forms a complex structural corridor that persists along strike for ~350 km to the northeast, including rocks mapped as Neuvo Segovia schist. The fold-and-thrust belt, although initiated in the Cretaceous, likely experienced episodic to progressive deformation until ca. 35 Ma (Rogers et al., 2007b) as a result of Caribbean tectonic reconfigurations (Rogers et al., 2007a; Andjić et al., 2019; Gazel et al., 2021). The Guayape fault system (Fig. 2A), approximately 30 km to the northwest of the Colon fold-andthrust belt, records middle Cretaceous left-lateral motion on basin-bounding faults (Silva-Romo, 2008).

A broadly NE-striking suite of middle Cretaceous-Paleocene felsic to intermediate batholiths are located along the western side of the Dipilto terrane and a few tens of kilometers east of the Guayape fault system (Figs. 1B, 2A). These include composite granitoids (tonalite, granite, and granodiorite) that form the 119 to 113 Ma Dipilto batholith (Garcia-Amador et al., 2019). This calc-alkaline, subduction-related batholithic complex intrudes the Nueva Segovia schist and is

best exposed along the Honduras-Nicaragua border, ~5 km northwest of the San Albino deposit (Fig. 2A; Burianek and Dolnicek, 2011; Garcia-Almador et al., 2021). Uranium-Pb dates on zircon from the calc-alkaline, ilmenite-series plutons closest to San Albino are ~113 Ma (Garcia-Almador et al., 2019). The intrusions are interpreted to have been emplaced at about 6-km depth (Burianek and Dolnicek, 2011) during the final stages of Mesquito terrane accretion and were rapidly exhumed in the late Albian (~110–105 Ma), a few million years after emplacement (Garcia-Almador et al., 2019, 2021). The thermal metamorphic aureole around the batholith overprints an Early Cretaceous greenschist facies regional metamorphic event and is associated with proximal andalusite and chlorite porphyroblasts (Burianek and Dolnicek, 2011). Outside of this aureole, the metasedimentary rocks primarily contain muscovite, chlorite, quartz, albite, and graphite, similar to the assemblages observed at the San Albino mine, indicating that the deposit occurs outside of the metamorphic halo to the Dipilto batholith. It has been suggested that the gold deposits in the region are related to batholith emplacement (Venable, 1994), but there is no direct evidence of a magmatic-hydrothermal or temporal association.

The area centered around the Dipilto batholith has been referred to as the Telpaneca-Murra-Macuelizo mineral district (Arengi and Hodgson, 2000), but it contains no significant historical production of base or precious metals. Numerous very small historical workings on orogenic gold-bearing veins in the Nueva Segovia schist define a 28- × 5- to 10-km NNE-striking belt termed the Corona de Oro gold belt (Fig. 2B) by present-day explorationists. The largest recognized of these historical occurrences was the San Albino lode deposit, which is now being exploited by a modern open-pit mine and is the subject of this study. The Corona de Oro gold belt represents a favorable target area for discovery of additional gold resources.

San Albino Geology

Host rocks

The metasedimentary Nueva Segovia host rocks to the San Albino orebody primarily consist of a strongly deformed,

Table 1. Comparison of the Geologic Characteristics of Major Low-Angle, Thrust-Related Orogenic Gold Deposits

		0		I		
Deposits	Vein dip, stacking, and style within shear zones	Vein/ore zone dimensions	Vein composition and alteration	Vein structures	Thrust ramps and anticlines	Ore age
San Albino Nicaragua	Shall. dipping ~30° stacked lam. shear veins along graphitic szs	Avg 1.2 m thick, avg zones 200 m strike and >400 m downdip	Qtz cal/ank plag (alb?) py, aspy, gal, sphal (cp, tm, rut); dark carbo- nac. seams of chl, ser; sulf ≤3%; W ≤500 ppm (scheel?)	Folds, boudins, breccias, stylolites	Tilted dome-like geometry	Albian (112–99 Ma)?
Macraes New Zealand	Shall. dipping stacked veins; two vein types both lam.; dominant subvertical stwk of originally extensional quartz veins; occas. shear veins along graphitic thrust planes	Avg 2–8 m thick; zones <2,000 m strike and 1,500 m downdip	Stwk veins: Qtz, mus, sid, scheel, cal, rut, gold, py, aspy; shear veins: dark seams of qtz, graph, py, aspy, gold (gal, sphal); Cu; W ≤1,000 ppm	Folds, boudins, breccias, minimal stylolites	Ore related to frontal and lateral thrust ramps	142–135 Ma
Paracatu Brazil	Shall, dipping single 100- to 140-m-wide high strain zone containing vein boudins along graphitic layers; mainly lam. shear veins and occas, extensional veins	Avg veins 2 cm thick; ore zone 100–140 m thick; 3,000 m strike and 4,000 m downdip	Qtz, aspy, ank, py, po, gal, sphal; cp, carb; carbonac. seams with sulfides; large qtz vein boudins with euhed aspy with gold inclu- sions; Ag, Sb, Bi, Ba, K, Cd; occas W	Folds, boudins, breccias, and stylolites	Footwall high causing thrust ramping beneath entire orebody	Early Braziliano (680 Ma)
Pogo USA (Alaska)	Shall. dipping, stacked veins along graphitic or serpentinite shear surfaces; mainly lam. shear veins and occas. steep extensional veins as offshoots from shear veins	Liese vein avg 3 m thick (0.3–10 m); 500 m along strike and 1,700 m downdip	Liese qtz veins with bi, ser, serp, carb, ~3 % py, po, loll, aspy, cp, gal, bism, mald, gold; some Te, Mo, and W	Folds, breccias, and stylolites; boudins not mentioned	Not described in literature	10 4 Ma
Nalunaq Greenland	Shall. dipping (36°) stacked veins within sz along contact between basalt and dolerite; lam. shear veins and occas. steep extensional veins as offshoots from shear veins at boudin necks	Avg <1 m (0.5–2 m); zones 400 m strike and 750 m down plunge	Qtz, diop, Ca plag, epid, gar, ank, ser, tm, py, po, sph, loll, aspy, mald, scheel, gold; drk seams of diop; Minor Cu	Folds and boudins	Not described in literature	1783–1762 Ma
Phuoc Son Vietnam	Shall. dipping stacked veins; lam. shear veins parallel sz foliation in sheath fold environment; occas. extensional veins	Avg 2.6 m thick; 500 m along stike and 1,500 m downdip	Qtz, bi, mus, ser, serp, py, po, carb, sphal, gal, gold (scheel, cp); 0.6% Pb; 0.25% Zn; no aspy	Folds, boudins, breccias, no stylolites mentioned	Not described in literature	Triassic (250– 200 Ma)
Bong Mieu Vietnam	Shall. dipping (20–40°) stacked shear veins along szs	Few cm to 11 m thick; zones of 2,000 m along strike and 2,000 m down plunge	Qtz, ser, clinoz, bi, epid, chl, carb, py, po, gal, sphal, aspy, bism, gold, moly, scheel, cp, fluor, tm	Folds, boudins, breccias, no stylolites mentioned	Deposits lie in the core and on either limb of anticline	~200 Ma
Crixas Brazil	Shall. dipping (~35°) stacked mineralized veins; mainly lam. shear veins along graphitic szs; three veins styles: massive sulfide, lam. qtz vein with dissem. sulfide, and sulfide-poor qtz veins; occas. steep extensional quartz veins as offshoots from boudin necks	Avg 1.5 m (0.5–5 m); 2,000 m along strike and 3,000 m down plunge; sheath fold environment	Chl, cal, bi, dol, aspy, cp, po, gal, pent, gold (plus Bi and Te min- erals); Ag. no W	Only folds and boudins mentioned	Deposits in an anticlinorium centered above basement Archaean dome	2137 Ma

Table 1. (Cont.)

Deposits	Host rock and age	Host-rock meta- morphic facies	Extent of occurrences	Au endowment and grade	Metallurgy	References
San Albino Nicaragua	Middle-Late Jurassic metapelites, graphitic schists	Greenschist	28 km of high- grade gold showings	0.28 Moz; o/p 9.1 g/t fully diluted; u/g 10.3 g/t	Grav. recov. 28–50%; balance CIL recov.	INETER (1995), Burianek and Dolnicek (2011), J.G. Payne (unpub. report, 2011), Lipson and Pudar (2016), Ristorcelli et al. (2020), Squires et al. (2022)
Macraes New Zealand	Permian to Late Triassic schists, metapelites and metapsammites	Greenschist	~20 km of mines and occurrences	>10 Moz; o/p 0.82 g/t M+I; u/g 2.59 g/t M+I	Mainly dissem. refrac. gold in sulfide; floatation then press. ox.	Teagle et al. (1990), MacKenzie and Craw (1993), de Ronde et al. (2000), Craw (2005), Begbie and Craw (2006), Mortensen et al. (2010), Redden and Moore (2010), Mortimer et al. (2016), Allibone et al. (2017, 2018), Edwards et al. (2020)
Paracatu Brazil	~1000 Ma metapelites and metapsammites, graphitic phyllites, and bedded clastic- chemical sediments	Greenschist	Single deposit	16.6 Moz o/p at 0.42 g/t	92% free milling gold; grav. conc. of gold and sulfide then CIL	Freitas-Silva (1996), Martini (1998), Hanson (2006), Sims (2014, 2020), Oliver et al. (2015, 2020)
Pogo USA (Alaska)	Neoproterozoic to mid-Paleo- zoic para- and orthogneiss, graphitic schist, serpentinite, and amphibolite in ore-host- ing shear zone; Liese vein best continuity in paragneiss	Amphibolite	15 km of occurrences (Goodpaster to Spring)	>10 Moz u/g at 9.8 g/t	Grav. conc, gold, and sulfide flotation followed by CIP circuit	McCoy and Olsen (1997), Smith et al. (1999), Rhys et al. (2003), P. Jensen (unpub. report, 2010), Graham-Ruzicka (2014), Northern Star Resources Ltd (2020a, b), Thompson (2020), D. Larimer, writ. commun. (2022), J. Rogers, writ. commun. (2022)
Nalunaq Greenland	Paleoproterozoic tholeiitic basalt in F/W and dolerite in H/W, both altered to calc silicate	Greenschist to amphibolite	2 km	0.75 Moz u/g at 28 g/t	Coarse-grained free gold 80% gravity recov.	Kaltoft et al. (2000), Bell et al. (2017), Gilbertson et al. (2017)
Phuoc Son Vietnam	~500 Ma carbonaceous schist/ phyllite and metagabbro	Amphibolite	9 km	0.88 Moz o/p at 7.77 g/t	Grav conc., gold and sulfide flota- tion then intense cyanidization	Stevens and Fulton (2008), Manaka et al. (2010), Manaka (2014), Tran et al. (2014)
Bong Mieu Vietnam	Mid-Paleozoic(?) metapelites and metapsammites, and lesser calc silicates after carbonate-rich rocks; also endoscarn	Amphibolite	6 km	0.83 Moz; o/p 2.43 g/t; w/g 7.8 g/t	Maily free gold; grav. conc., gold, and sulfide flota- tion then intense cyanidization	Stevens and Fulton (2009), Tran et al. (2014)
Crixas Brazil	2.28–2.26 Ga schistose graywacke and graphitic phyllite thrust on top of Mesoarchaean	Mainly greenschist; local amphibolite	3 km	8.3 Moz u/g at 5.5–8.3 g/t	58% Au captured as grav. conc; remain- der captured in CIL plant	Jost and Fortes (2001), Jost et al., (2010), USGS (2016), AngloGold Ashanti Ltd (2021), Bogossian et al. (2021), Borges et al. (2021), R.G. Souza (writ. commun., 2021), Ulrich et al. (2021)

Abbreviations: alb = albite, ank = ankerite, aspy = arsenopyrite, avg = average, bi = biotite, bism = bismuthenite, cal = calcite, Ca plag = calcite plagioclase, carb = carbonate, carbonate = carbonate ceous, chl = chlorite, CIL = carbon in leach, clinoz = clinozoisite, cp = chalcopyrite, dep = depositional, diop = diopside, dissem. = disseminated, dol = dolomite, drk = dark, epid = epidote, euhed = euhedral, flour = flourite, F/W = footwall, gal = galena, gar = garnet, graph = graphite, grav conc = gravity concentration, H/W = hanging wall, lam = laminated, loll = lollingite, M+I = measured + indicated, mald = maldonite, moly = molybdenite, Moz = million ounces, mus = muscovite, o/p = open pit, occas = occasional, pent = pentlandite, plag = plagioclase, po = pyrrhotite, press ox = pressure oxidation, py = pyrite, qtz = quartz, recov = recovery, refrac = refractory, rut = rutile, scheel = scheelite, ser = sericite, serp = serpentinite, shall = shallow, sid = siderite, sph = sphene, sphal = sphalerite, stwk = stockwork, sulf = sulfide, sz(s) = shear zone(s), tm = tourmaline, u/g = underground

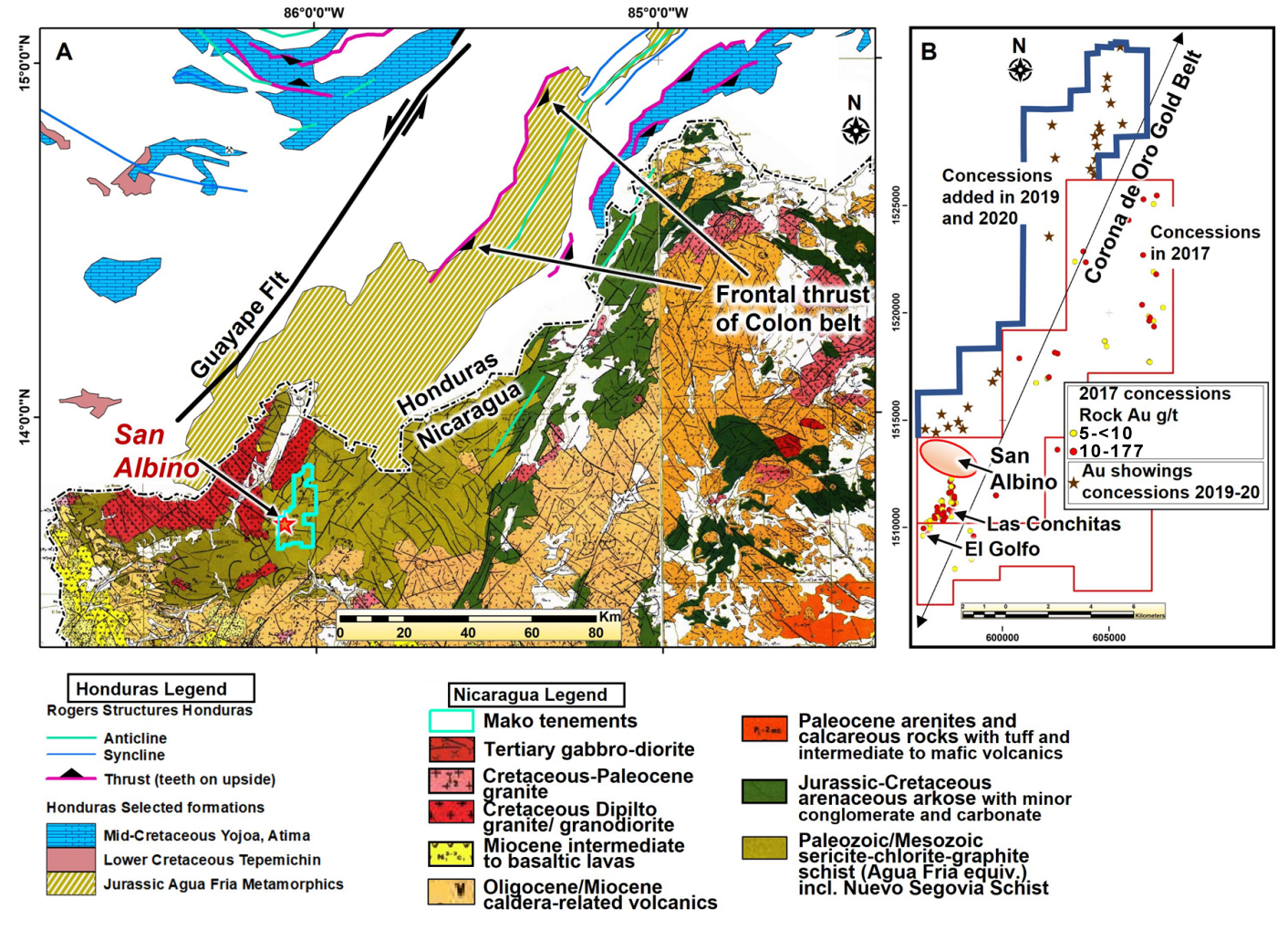


Fig. 2. A. Geologic map displaying the geology of Nicaragua derived from Instituto Nicaraguense de Estudios Territoriales (1995) with selected geologic formations in Honduras from Rogers (2003). B. Gold showings and high-grade gold grab samples along \sim 30 km of strike length, defining the Corona de Oro gold belt. Flt = fault.

green to brown graphitic schist, which contains compositional layering defined by quartz-rich, quartz-muscovite (±tourmaline), and carbonaceous layers. These variably contain iron oxide-rich layers that comprise hematite and secondary hydrated iron oxides. Less common is a foliated green to brown chloritic phyllite. Because of deformation and metamorphism, bedding is not recognizable in the immediate host rocks to the San Albino deposit, although a rare outcrop with preserved bedding, defined by psammitic layers parallel to foliation of the enclosing pelitic schist (Fig. 3A), is exposed south of the mine at Las Conchitas (Fig. 2B). Consequently, attempts at establishing a local stratigraphy on a visual, structural, or geochemical basis have thus far been unsuccessful. The deformation fabric of the ore host rocks is detailed below.

The metasedimentary rocks and mineralized quartz veins are cut by a series of predominantly subvertical andesite dikes. The mainly ESE-striking dikes display sharp contacts with the schist and mineralized quartz veins, which they cut (Fig. 3B, C). They do not, however, displace mineralization to any significant extent (Fig. 3B). Minor sills are also present. The dikes contain hornblende, quartz, and plagioclase

phenocrysts with hornblende completely altered to intergrowths of calcite, chlorite, quartz, and ilmenite/leucoxene, while plagioclase phenocrysts are largely altered to fine-grained muscovite (i.e., sericite). Similarly, the plagioclase and hornblende groundmass is altered to muscovite, ankerite, and calcite with hydrated iron oxides and minor chlorite and quartz. The intense nature of mineral breakdown, which appears restricted to the dikes themselves, indicates post-ore alteration. The dikes have finer-grained chilled margins along contacts with schist, but the dikes lack any structural fabric. Drill assays from dike intersections rarely contain gold. Pyrite, minor chalcopyrite, and ankerite have been locally observed along dike-schist contacts, and it is uncertain whether they relate to the earlier gold-forming event.

The schist also hosts abundant small (cm-scale), elongate, folded, or boudinaged nonmineralized quartz pods and veins. These are considered to have been more continuous veins formed during early metamorphism prior to the onset of the Colon folding and thrusting events. These veins are milky white, largely monomineralic, and barren. These likely represent colloidal silica, which was expelled from precursor

clay-rich sediments at diagenetic temperatures below 200°C as local metamorphic amorphous silica gels (e.g., Elliston, 2018).

Deformation and fabric relationships

The Nueva Segovia schist in and surrounding San Albino displays ubiquitous foliations, the earliest of which (S_1) is attributed to one or more premineral deformation events (D_1) . A secondary S₂ foliation is developed along F₂ fold axial planes in tightly folded early, nonmineralized quartz veins (Fig. 4A) and in isoclinally folded S₁ foliation in schist (Fig. 4B). The difference between S₁ and S₂ can only be identified in the hinge zones of F₂ folds because elsewhere these two foliation sets are further dragged into parallelism during a D₃ shear event, forming an S_3 fabric. This S_3 is identified along the boundaries of mineralized breccia veins as described below. Consequently, the dominant schist fabric that reflects all three deformation episodes is hereafter referred to as S_D. Detailed studies of the schist are limited to observations in close proximity to mineralized quartz veins where deformation is particularly intense and S/C structures are commonly developed (Fig. 4C). As described below, the alteration zones adjacent to gold-bearing quartz veins also have an S/C fabric.

The structural framework is predominantly derived from foliation and quartz vein geometries because primary stratigraphical relationships are not preserved. Data collected on surface prior to current mining operations are plotted at two scales: first from the immediate San Albino mine area (yellow box, Fig. 5A) and then from a wider area that includes Las Conchitas to the south (red box, Fig. 5A). In general, the dominant foliation (S_D) dips ~30° toward the northwest, although a subordinate subset of foliation measurements dips toward the southeast (Fig. 5C, D), likely due both to folding and to locally incomplete transposition of $S_{1/2}$ into S_3 . In the San Albino mine area, poles to the NW-dipping foliation (S_D) produce an average plane that strikes 185° (right-hand rule) and dips 25°, and the SE-dipping foliation strikes 070° and dips 20° (Fig. 5C). The resultant fold hinge lines deduced from these two sets of oppositely dipping foliation planes plunge 213°/12° (Fig. 5C), similar to the trends observed in the broader study area (Fig. 5D). The widespread occurrence of S/C structures in which the S fabric dips more steeply than the C fabric (Fig. 4C) further contributes to scatter in the S_D foliation measurements.

In plan view, variations in foliation orientations define a dome-like antiformal culmination (Fig. 5B, black ellipse) along a major anticline (Fig. 5B, thick purple line). Small-scale parasitic folds on both limbs of the anticline are deduced from the data. These display fold hinge lines with shallow plunges toward the southwest, although a subordinate set display northeast plunges. In part, this may result from the parasitic folds being variably oriented surrounding the central part of the domal culmination (Fig. 5B).

Mineralized quartz veins

The three main mineralized quartz vein sets developed at the San Albino deposit are named San Albino at the shallowest level, Naranjo at an intermediate depth, and Arras at the greatest depth (Fig. 6A). All these quartz vein sets continue to surface and display graphitic slicken surfaces along their margins, suggesting that they lie along shallowly dipping shear planes. Based on stereographic analysis of the mineralized vein sets, their average strike and dip is $230^{\circ}/35^{\circ}$ (right-hand rule) (Fig. 5E), although a subordinate proportion of measurements dip at low to moderate angles toward the southeast. Surface outcrop measurements of quartz vein attitudes largely agree with the quartz vein dips deduced from drilling, i.e., 20° to 35° to the northwest (Fig. 6A). Also, the veins broadly parallel S_D (Fig. 5C-F). The sheet-like vein-hosting shear planes are more continuous than the enclosed quartz veins, and together they provide the basis for vein correlations (Fig. 6A). The discontinuous nature of mineralized veins is also apparent in outcrop (Fig. 5B) and in the plan projection of ore blocks (Fig. 6B).

The San Albino vein set has been deformed and disrupted by reverse movement (NW over SE; D_3) as indicated by the asymmetry of an anticlinal F_2/F_3 fold and by the sense of reverse fault thrust duplication in the breached antiform (Fig. 6A). Fold thickening in the hinge zone and the duplication result in an unusually wide (~5–8 m) composite vein zone. Thrust propagation along foliation and fault breakthrough may have been the result of progressive shear and/or a separate event. The mineralized veins are further affected by later brittle faults (e.g., the Mine Creek fault zone; Fig. 6A). These appear to be subvertical, NE-striking faults, marked by discrete gouge zones, and they locally bring the downdip portion of veins closer to surface.

The anticline depicted in cross section (Fig. 6A), which deformed the San Albino vein set as defined by drilling, represents the same dominant anticline depicted on surface in Figure 5B. The mineralized part of the anticlinal axis from section to section can be traced for at least 100 m along an azimuth of 045° at a plunge of 14° and thus shallowly toward the northeast. Plunges to both the northeast and the southwest are anticipated from the described domal geometry. In broad outline, the folding deduced from all the stereographic projections indicates almost horizontal, SE-plunging fold axes with an azimuth and plunge of roughly 200° and 10°, respectively.

The typical broad agreement between the orientation of veins and schist fabric can also be seen at the outcrop scale (Fig. 7A, C), although in places veins crosscut the foliation (Fig. 7B). Quartz veins predominantly lie parallel to the schist C fabrics but may locally follow the S fabrics, as seen in both the Arras vein set and in the upper parts of the San Albino vein set (Fig. 8A, B). Progressive deformation with synthrust folding of mineralized quartz veins is commonly observed in the San Albino deposit (Fig. 8C). Where deformation is most intense, the narrower veins (5–20 cm thick) are locally isoclinally folded (Fig. 8D).

The San Albino, Naranjo, and Arras mineralized vein sets are each separated by an average vertical distance of 90 m (Fig. 6A) (Ristorcelli et al., 2020), suggesting that the broad domain that accommodated shear-related vein emplacement is, at a minimum, ~180 m wide. The mineralized quartz vein sets display an average thickness of 1.2 m (Ristorcelli et al., 2020; this study) (Fig. 7) and are host to discontinuous, discrete ore shoots that are roughly aligned in two orthogonal directions: downdip and along strike (Fig. 6B). These are further complicated by local folding, thrust disruption, and/or

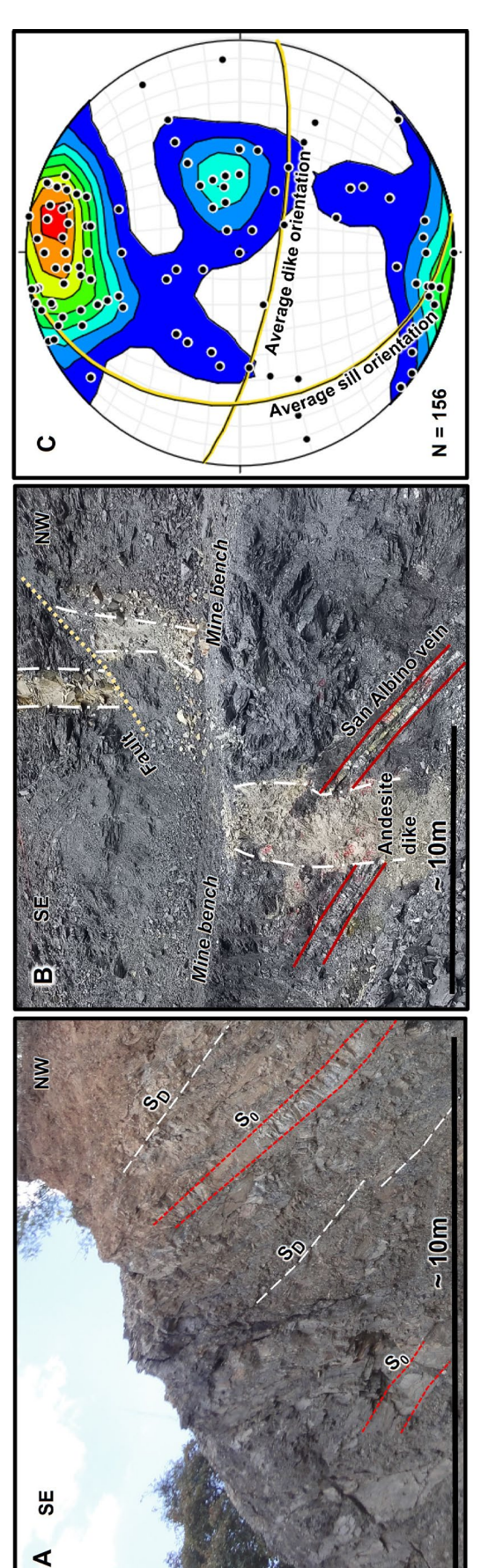


Fig. 3. A. Field photograph of an outcrop exposure from the Las Conchitas area that preserves rare psammite bedding markers (So). B. Field photograph of an andesite dike with sharp contacts that crosscuts both foliation and the mineralized San Albino vein set. Dike is itself displaced by a later normal fault. C. Equal-area, lower-hemisphere projections of poles to dikes and sills. Average dike strikes 100° and dips 76° south-southwest, average sill orientation is 170°/30° (strike/dip)



matic indicators and showing coeval development of an axial planar cleavage (Lipson and Pudar, 2017). B. Photograph of a thin section that contains tight folds in graphitic schist with graphite seams both along So₁₁ layers and foliation and redistributed as S₂ along D₂ fold axial planes. C. A photomicrograph of strongly deformed schist that occurs proximal to the San Albino vein set showing S/C fabrics defined by quartz-rich (qz) bands and those dominated by coarse- and fine-grained muscovite (mu/se) with Fig. 4. A. Field photograph of a partially preserved Z fold defined by an unmineralized quartz vein from the Las Conchitas area. Southeast vergence deduced from kineseams of abundant carbonaceous material (co). Zr = zircon.

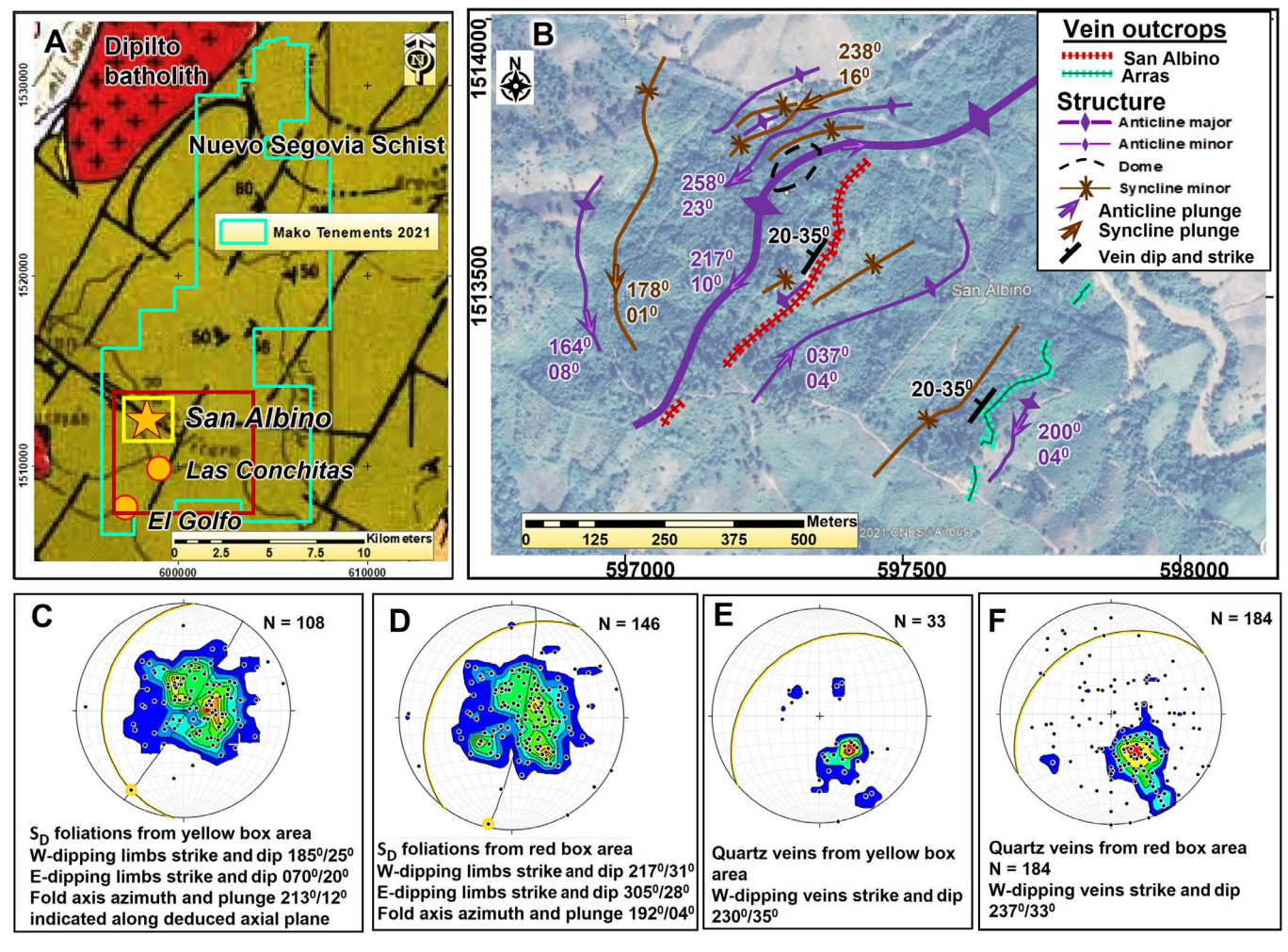
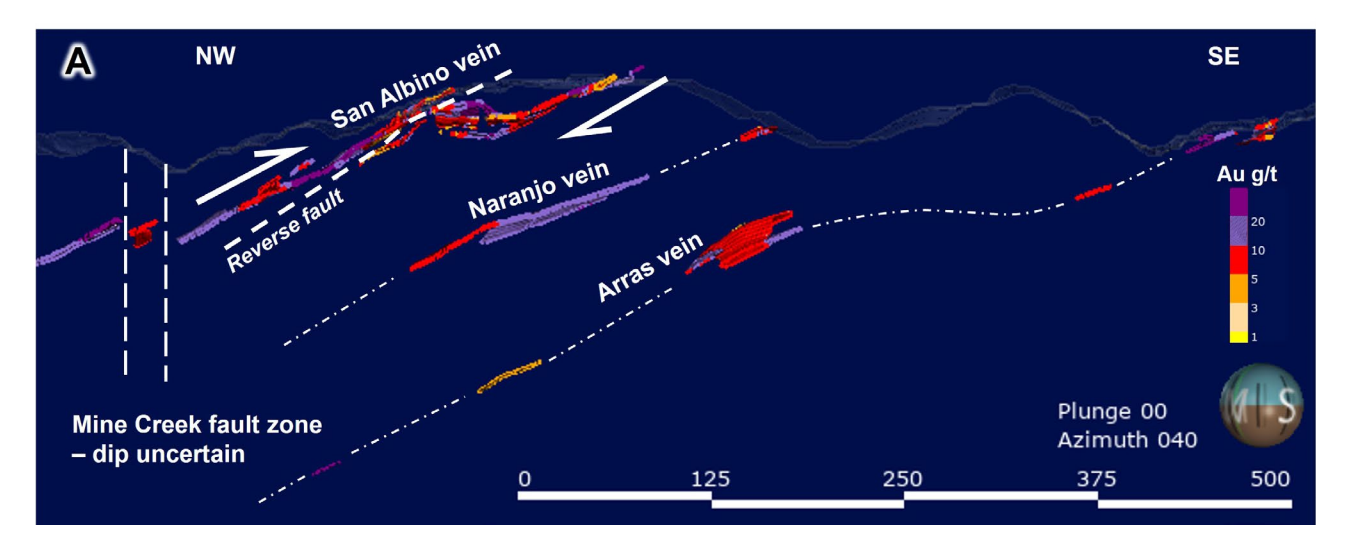


Fig. 5. A. Map displaying the location of Mako Mining tenements and two data domains. Yellow domain for mine data plotted in C and E is a subset of the more regional red domain data plotted in D and F. B. Satellite image of the San Albino deposit area prior to mining annotated with exposed vein sets, and the axial trace of large-scale folds interpreted from foliation measurements. C-F. Equal-area, lower-hemisphere projections of poles to foliation (C, D) and quartz veins (E, F). Data from mine personnel and authors.

boudinage, as described below. Based on the block model by Ristorcelli et al. (2020), which usually includes a rind of lowergrade gold-bearing graphitic rock 0.5 m above and below the veins, orebody thicknesses vary from 1 to 8 m (Table 2). The thickest parts are located in areas of vein duplication resulting from folding and/or thrusting (Fig. 6A). The most continuous of the three vein sets is San Albino with the largest vein continuing for at least 650 m downdip and ~300 m along strike (Fig. 6B). The San Albino vein set also has a second zone of continuous mineralization with strike and dip extents of the gold-bearing vein of 160 and 140 m, respectively. The San Albino vein set broadly displays an inverse relationship between vein thickness and gold grade, particularly above a 15-g/t Au threshold, but there are many exceptions to this generalization (Fig. 9), as would be anticipated in a multiply deformed orebody. Below 15 g/t Au, there is no clear relationship between gold and vein thickness, which may point to two distinct populations. The Naranjo vein set is the least well-developed of the three mineralized bodies, with one main continuous body measuring 230 m downdip and 90 m along strike. The Arras vein set is host to three continuous orebodies, with the largest measuring 550 m downdip (but still open in that direction) and 120 m along strike, whereas the other two bodies are less coherent downdip but display good along-strike continuity. Vein thicknesses are highly variable, ranging from 1 to 8 m (Table 2). In addition, many other smaller pods occur (Fig. 6B). Separation of quartz veins into mineralized zones with downdip or down-plunge continuity exceeding along-strike continuity is a feature of all comparable ore deposits listed in Table 1, whether or not they display evidence of boudinaging. Hence, the San Albino deposit limitations on strike continuity of quartz vein ore shoots is unlikely to have been strongly influenced by macroscopic boudinage.

The mineralized quartz vein sets typically display laminations defined by lighter and darker bands of quartz with heterogeneously incorporated slivers of country rock (Figs. 7, 8), which provide further evidence for vein formation after D₁. Robert and Boullier (1994) attributed such vein laminations to incremental vein development with individual laminae separated by discrete slip surfaces or by slivers of foliated



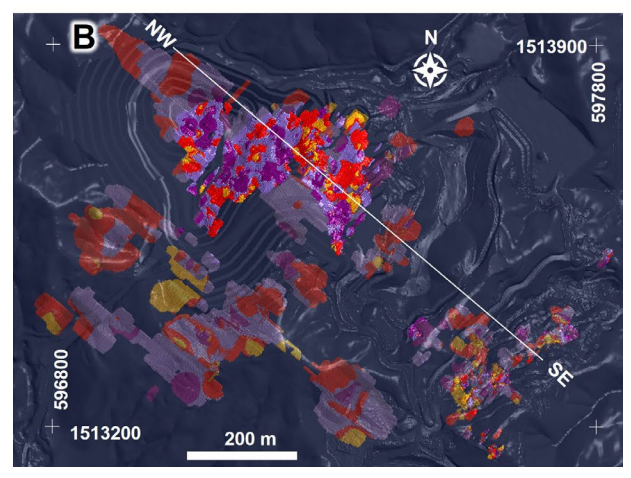


Fig. 6. A. San Albino deposit cross section showing measured, indicated, and inferred block model grades for all three veins as of mid-2020. Colors refer to grades as shown in legend. Over 90% of the grade in the deposit is contained in quartz veins; hence, the block model provides an accurate representation of the mineralized component of quartz veins. The dot-dash lines linking blocks reflect the shear surfaces along which both subeconomic and economic quartz veins are developed. The San Albino vein is deformed by an asymmetric F_2/F_3 anticline superimposed by a reverse fault duplex structure. Thickening occurs there as a result of both the folding and faulting. Later faults are indicated on the northwest side of the cross section. Section corridor is 25 m wide. B. Plan projection of block model for all three veins against a background of the open-pit mine plan as of mid-2020. Location of cross section in A is shown.

wall rocks. Recent mining operations have revealed examples where the mainly concordant largest San Albino vein (Fig. 7A) locally has a crosscutting relationship to the foliation (Fig. 7B), indicating that mineralization postdated the D_1 and possibly later fabric-forming events. The presence of folded and thrust-duplicated mineralized vein sets suggests that mineralization occurred during an intermediate stage of a progressive deformation event (e.g., D_2 through D_3). These sets also lie along the major shear zone(s) further indicating that they developed during a regional contractional event.

Boudins

Boudinaging occurred during at least two deformational events, an early premineralization event and one that post-dates mineralization. In the Las Conchitas area 2.5 km to the southeast of San Albino where small-scale nonmineralized quartz vein boudins are abundant, the shear S fabric shown in Figure 8E rises from below one extremely stretched boudin to above the next, indicating a shear event (D_2/D_3) that post-dated the original extensional event that formed the boudins. This early extensional event thus predates both mineralization as well as the extensional event that caused boudinaging of mineralized quartz veins.

Boudinging of gold-bearing veins by definition postdates the D_2/D_3 mineralizing event (see below) and occurs both

along fold limbs (Fig. 8F) and as disaggregated mineralized quartz veins of up to 1 m in thickness commonly observed at the San Albino mine and as far removed as 20 km to the northnortheast. At Las Conchitas, incipient development of boudins (Fig. 8G) or complete boudinage of mineralized quartz veins is commonly developed. Chocolate tablet boudinaging of 1- to 1.5-m-thick mineralized quartz veins is also observed there. This is a feature interpreted by Robert and Poulson (2001) to be indicative of extension in two orthogonal directions resulting from bulk flattening within the host shear zone.

Breccias

Brecciation is a common feature associated with mineralized quartz veins at San Albino. Preexisting D_2 quartz veins with slivers of schist that help define the laminations are fragmented during D_3 development of S/C structures, and sulfides together with possible dark quartz help define the new S fabric, forming a matrix to the D_2 quartz vein clasts. Clasts vary in shape from angular through subrounded to rounded, and stoping of earlier quartz vein material is evident along the sidewalls of the sulfide-rich veins (Fig. 10A, E). The sulfides, and thus coeval gold, form shear veins crosscutting D_2 quartz vein laminations (Fig. 10A) and are intimately associated with the breccias, suggesting that sulfide with gold was introduced during D_3 , a brittle-ductile event. At the Macraes deposit in

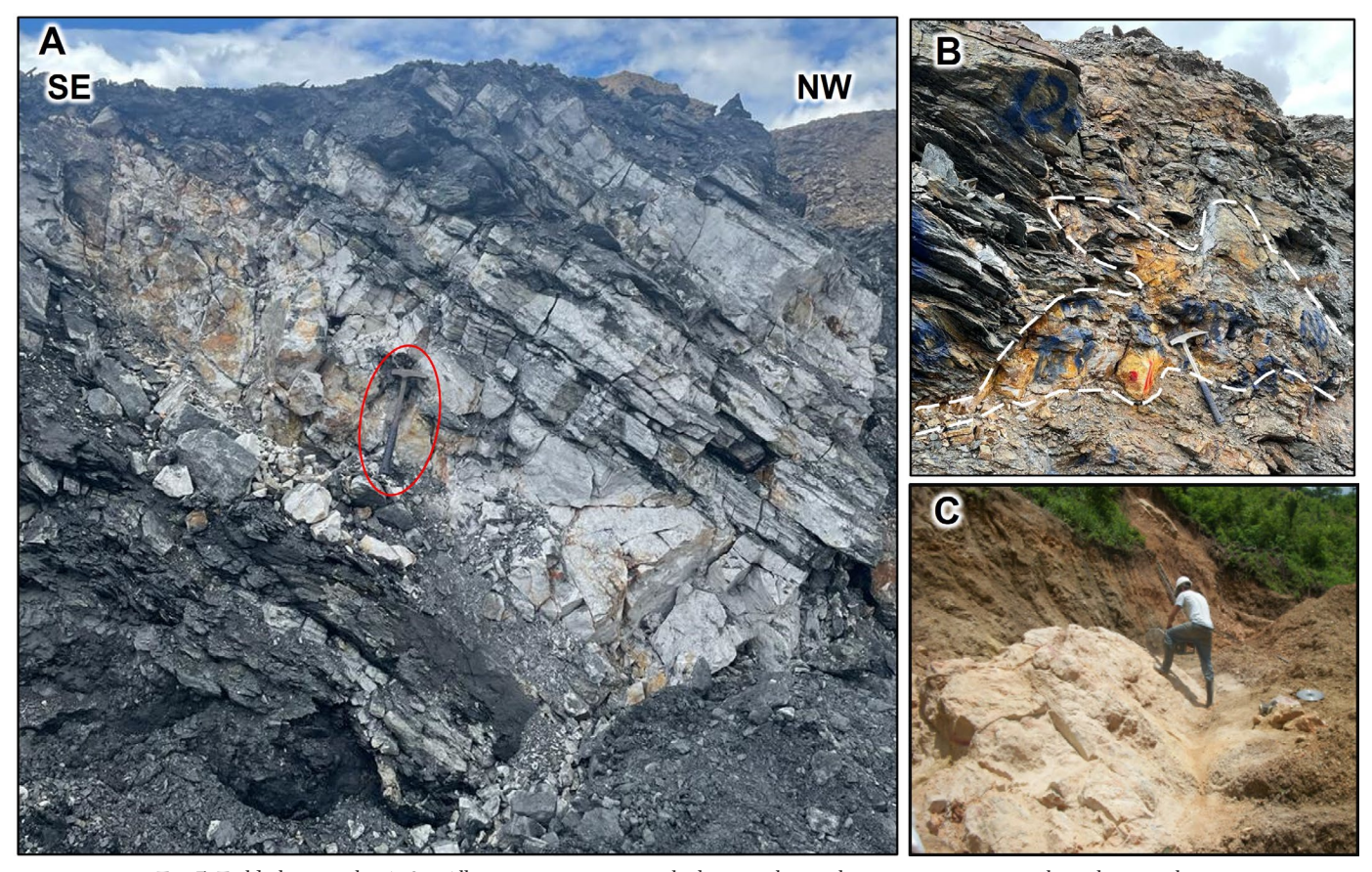


Fig. 7. Field photographs. A. San Albino composite vein set looking southwest showing a massive central part between laminated quartz veins lying parallel to host-rock foliation. Note hammer for scale. B. Complex San Albino vein set partly crosscutting (and postdating) the early host schist foliation. C. Massive Arras vein looking northeast with Zoran Pudar standing on scarp slope. Photos A and B courtesy of Frank Powell and Zoran Pudar.

New Zealand, Teagle et al. (1990) similarly described mineralized quartz veins that follow S fabrics developed during low-angle thrusting and along which localized pods of brecciated quartz veins are developed as implosion breccias because of localized pressure release.

In an example of where a brecciated quartz vein with abundant sulfide matrix abuts a fault breccia, the fault, which is essentially unmineralized, comprises a weakly foliated graphitic gouge that envelops quartz clasts of various sizes. The graphite fabric and larger quartz vein clasts parallel the margin of the quartz vein, suggesting that the fault breccia also formed during thrust-related shearing (Fig. 10B-D).

Stylolites

Stylolites are present as thin wavy bands with a mean planar surface lying subparallel to the laminations within the quartz veins (Fig. 11A, B). They comprise concentrations of auriferous fine-grained pyrite (Fig. 11C, D) and arsenopyrite (Fig. 11E, F) that were localized along the laminations during progressive deformation. Stylolites generally develop along a plane perpendicular to σ_1 as a result of pressure solution, with the up and down perturbations parallel to σ_1 (Sibson, 1994), and they effectively reflect flattening. Pressure solution occurs by dissolution of minerals at grain-to-grain contacts into an aqueous pore fluid under high stress and rising temperature until close to the critical point of pure water

 (374°C) , when retrograde quartz solubility occurs (Monecke et al., 2018). Although laminations are present in brecciated D_2 quartz vein clasts within sulfide matrices (Fig. 10), stylolites have not yet been recognized there. This might indicate that the pressure solution flattening, which caused stylolite development, occurred during the latter part of the mineralizing history. The high gold grades associated with stylolites (Ristorcelli et al., 2020) suggest that the subvertical loading pressure necessary for creating stylolites concentrated gold from within preexisting gold-bearing veins. This loading, which likely also created or accentuated boudin development, is addressed below.

Ore zone mineral and geochemical characteristics

For mining purposes, mineralization is divided into oxide, mixed (transition), and fresh (hypogene) zones. The oxide zone extends from surface to between 20- and 30-m depth, with a ≤5-m-thick mixed zone. Low sulfur values augment visual recognition of oxide and mixed zones where they are an order of magnitude lower than in the hypogene mineralized zone (Ristorcelli et al., 2020). Indicated resource oxide gold grades are depleted relative to hypogene values (6.21 vs. 9.17 g/t), but with little change in silver values (Puritch et al., 2015). In the hypogene zone, gold mineralization occurs primarily in association with sulfides within and along the margins of quartz ± carbonate (calcite ± ankerite) veins. The

Table 2. The Thickness and Size Parameters for Major Ore Shoots in Vein Sets of the San Albino Deposit Based on the
2020 Resource Block Model (plus many other smaller surface areas of veins; Ristorcelli et al., 2020)

	Ore-shoot orientation NW (downdip)					Ore-shoot orientation NE (along strike)				
Name	Long axis (m)	Short axis (m)	Thickness avg (m)	Thickness max (m)	Thickness min (m)	Long axis (m)	Short axis (m)	Thickness avg (m)	Thickness max (m)	Thickness min (m)
San Albino Naranjo	650 235	300 90	2–4 2	6 3	1 1	160	140	2	4	1
Arras	550	120	2.5	6	1	330 320	170 120	2.5 2.5	8 5	1 1

Each of the veins tends to be at its thickest where the two ore-shoot orientations intersect; parameters used for block evaluations are intersection of >1 g/t Au and >1-m true width; mining model blocks typically encompass a mineralized quartz vein with an added 0.5-m rind both above and below the vein

highest gold grades are in veins with stylolites or with locally abundant galena grains (Ristorcelli et al., 2020). In drill core, galena, arsenopyrite, and visible gold are commonly observed together with lesser sphalerite. Sphalerite and arsenopyrite grains associated with mineralization commonly contain exsolution blebs of pyrrhotite and chalcopyrite, with the latter only observed in sphalerite.

Gold in quartz veins and associated sulfides is primarily free, occurring as native gold or electrum. Gold grains are also located along quartz grain boundaries and within microfractures and vugs (Fig. 12). Average gold grain diameter is 12 to 30 μm , but a significant proportion exceeds 30 μm , making gold amenable to gravity recovery (Ristorcelli et al., 2020).

In the San Albino deposit, silver and lead are strongly correlated (correlation coefficient >0.7), suggesting that silver resides in the galena lattice. For gold values up to 25 g/t, the Ag/Au ratio is roughly 2:1; above 25 g/t Au, there is no correlation and silver seldom exceeds 100 g/t, while many gold samples exceed 50 g/t. Lead also correlates reasonably well with gold up to 25 g/t Au with a correlation coefficient of 0.5, but above 25 g/t Au there is no correlation. The decoupling of gold from both silver and lead above 25 g/t Au and the good silver to lead correlation across their full data ranges strongly support earlier evidence for two gold events. The first appears to be a gold-only event, whereas the second has gold related to base metals and silver. Ristorcelli et al. (2020) note that drill samples with Pb >500 ppm average 4,365 ppm As, 0.8 ppm Hg, 6.6 ppm Sb, and 3.1 ppm Tl. Tungsten commonly occurs at elevated levels of up to 500 ppm and may indicate the presence of scheelite.

The carbon-rich selvages to the mineralized quartz veins host a lesser but important component of gold. While metallurgical recoveries based on optimized leach tests averaged 86.1% for sulfide ore including gravity recoveries of 36.3% (Ristorcelli et al., 2020), the main factor preventing higher recoveries is preg-robbing carbon. However, implementation of rigorous grade control measures coupled with careful blending of carbonaceous and noncarbonaceous ore to the mill has mitigated this problem, resulting in more consistent recoveries in the low- to mid-80% range. More detailed studies are needed to address the source and characteristics of the preg-robbing carbon. A previously unrecognized style of high-grade silver mineralization recently intersected in many drill holes at Las Conchitas, occurs in 1- to 3-m-wide fracture zones unrelated to quartz veins or alteration and with relatively no gold (Mako Mining, 2023a). These zones bear the

unusual geochemical signature of elevated tungsten (W >100 ppm), nickel, and copper, as exemplified by a 1-m interval located at a vertical depth of 123 m grading 3,792 g/t Ag with >1 % Cu and 0.13% Ni.

Alteration

A muscovite and fine-grained muscovite (sericite) mix with seams of abundant carbonaceous material frequently form the dominate selvage to quartz veins. However, in places the better-mineralized quartz veins of the San Albino deposit have a schist selvage alteration assemblage that includes fine-grained chlorite, partly to strongly granulated ankerite, calcite, and altered plagioclase (likely albite) with local tourmaline and rutile (Fig. 13A). Quartz in the mineralized veins was originally medium to very coarse grained but has been intensely deformed and recrystallized to much finer subgrained aggregates with sutured grain borders (Fig. 13A, C). This style of quartz vein is cut by a younger vein generation characterized by a similar but coarse-grained (up to 0.5 mm) alteration mineral assemblage of unstrained chlorite, ankerite, and quartz (Fig. 13B).

Along the margins of mineralized quartz veins, the earlier formed foliation is dragged against the vein, confirming that shearing persisted beyond at least the earliest mineralizing event (Fig. 13A). The strongly deformed alteration assemblage (Fig. 13C) further confirms the intense shearing that postdated the alteration (Fig. 13D).

Proximal mineralization

Mineralized veins are best understood in the San Albino deposit area where mining and the majority of recent exploration have occurred. However, NW-dipping, high-grade goldbearing veins with similar characteristics are observed for tens of kilometers along strike. These include veins in the Las Conchitas and El Golfo areas (Fig. 14), where near-mine exploration is ongoing, and those occurring for up to 20 km to the northeast of San Albino (Fig. 2B). Preliminary exploration at Las Conchitas has defined continuations of the stacked mineralized vein systems with the largest of these displaying downdip continuity of >200 m. Because the vein systems there also crop out at surface, they are likely to be amenable to open-pit mining, similar to the San Albino deposit. In addition to mining, exploration, resource definition, and feasibility assessment of this and other similar occurrences in the Corona de Oro gold belt are currently the focus of work conducted by Mako Mining Corp.

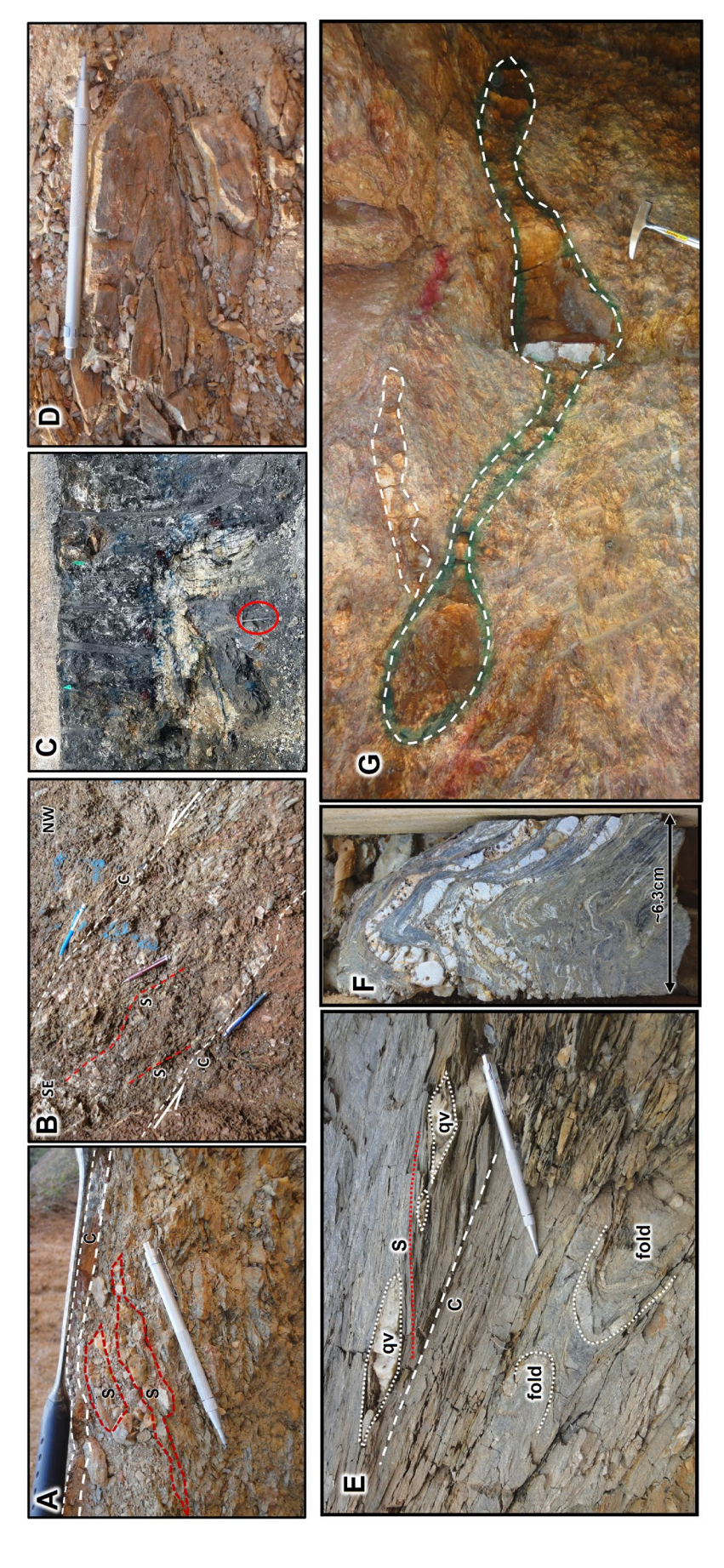


Fig. 8. A-E and G are field photographs. A. Arras vein set with internal strands following S (red highlighted) and C (white highlighted) structures. B. Upper part of San Albino vein set with C structures (white outline) bounding the set and with internal vein strands along S structures (red dashed lines). Sense of movement is northwest over southeast. C. Macroscopic folded San Albino vein set looking northeast (hammer for scale) (photo by Frank Powell and Zoran Pudar). D. Mesoscopic isoclinally folded top strand of Arras vein set. E. Las Conchitas postboudin S structure disruption (dotted red line) of the plane along which the unmineralized quartz veins to the left and below scribe. F. Drill core with folded San Albino quartz vein strands displaying boudins along the limbs. G. Mineralized quartz vein from Las Conchitas displaying incipient boudinage.

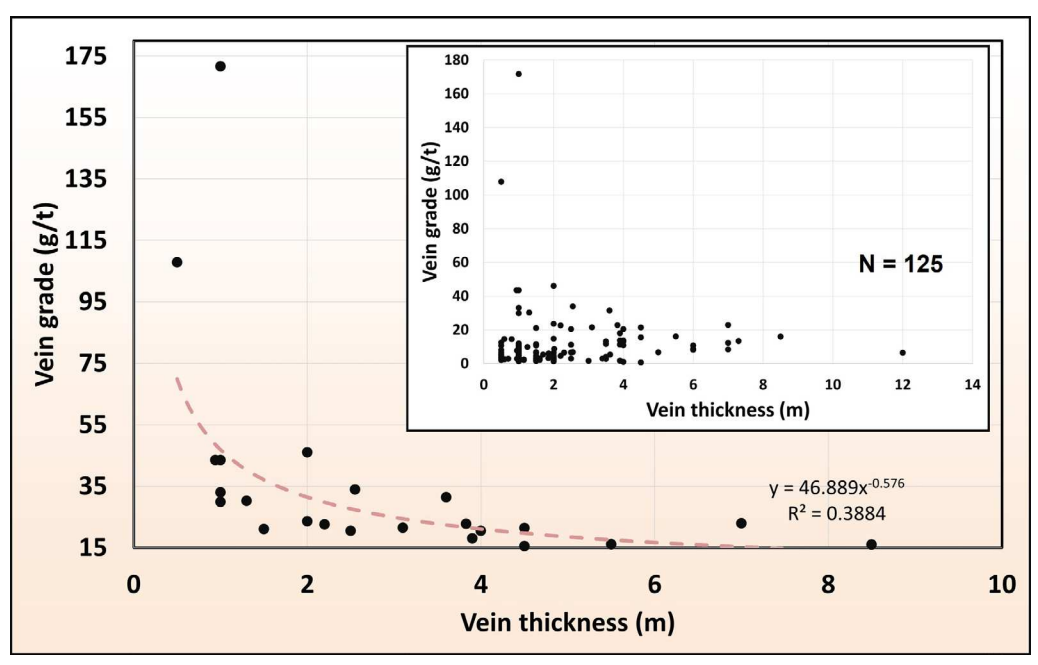


Fig. 9. Gold grade versus thickness for San Albino vein set. Above 15 g/t Au there is a clear power curve relationship. The inset shows the gold grade versus thickness plots for veins >0.5 g/t Au.

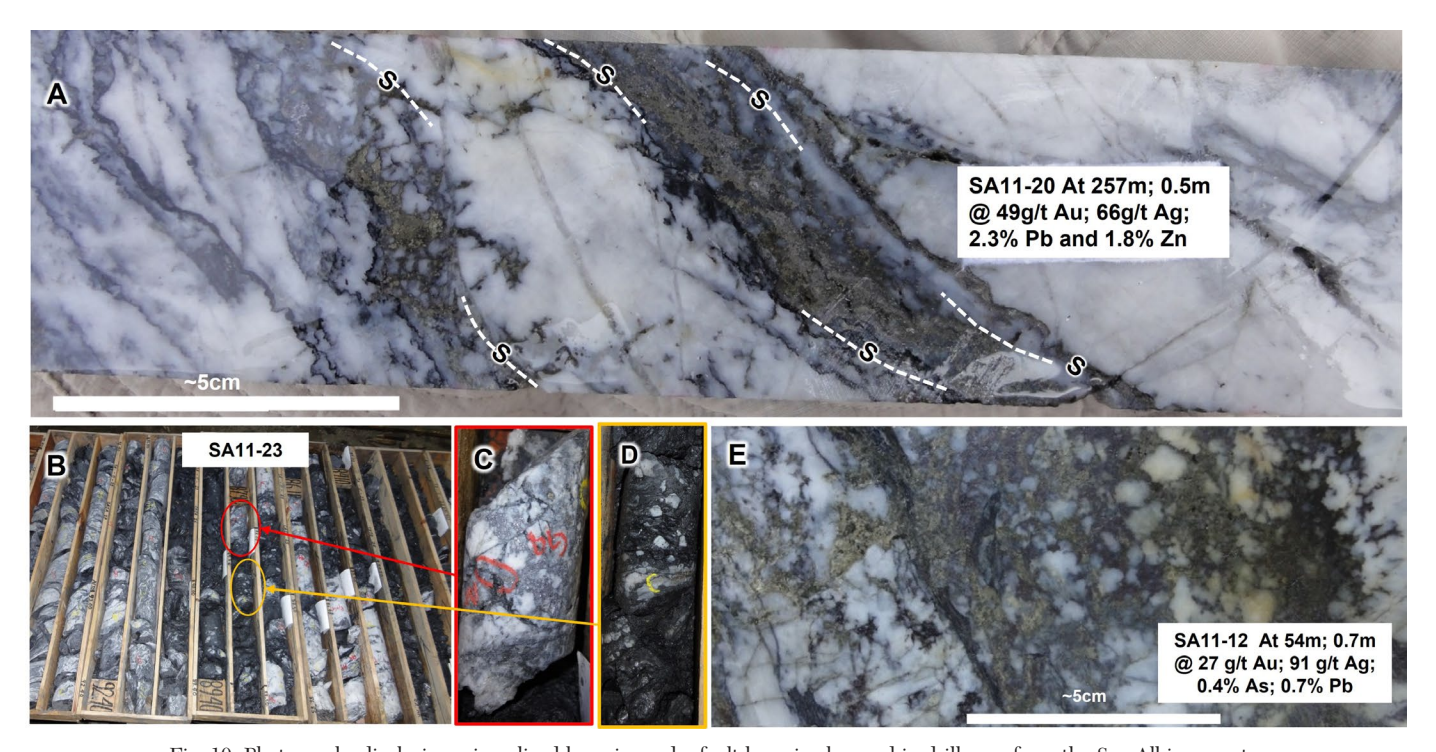


Fig. 10. Photographs displaying mineralized breccias and a fault breccia observed in drill core from the San Albino quartz vein set. A. Pyrite (plus galena and sphalerite) flooding and brecciation along S fabrics in earlier formed quartz veins. These surfaces along which D_2 quartz veins are disrupted are consequently termed S_3 . Kinematic movement right over left. SA11-20 at 257 m; 0.5 m at 49 g/t Au, 66 g/t Ag, 2.3% Pb, and 1.8% Zn. B. Box of drill core showing locations of base metal-rich interval (C) adjacent to barren fault breccia (D). C. Quartz vein breccia fragments in graphitic, sulfide-rich matrix adjacent to fault breccia (hole SA11-23 at 88 m). Galena and arsenopyrite are readily visible, and the interval has grades of 4.5 g/t Au, 15 g/t Ag, 954 ppm As, 0.7% Pb, and 0.3% Zn. D. Barren, sulfide-free fault breccia with quartz vein fragments in graphitic gouge. E. Pyrite-rich quartz vein breccia with unusually high Ag/Au ratio. SA11-12 at 54 m; 0.7 m at 27 g/t Au, 91 g/t Ag, 0.4% As, and 0.7% Pb.

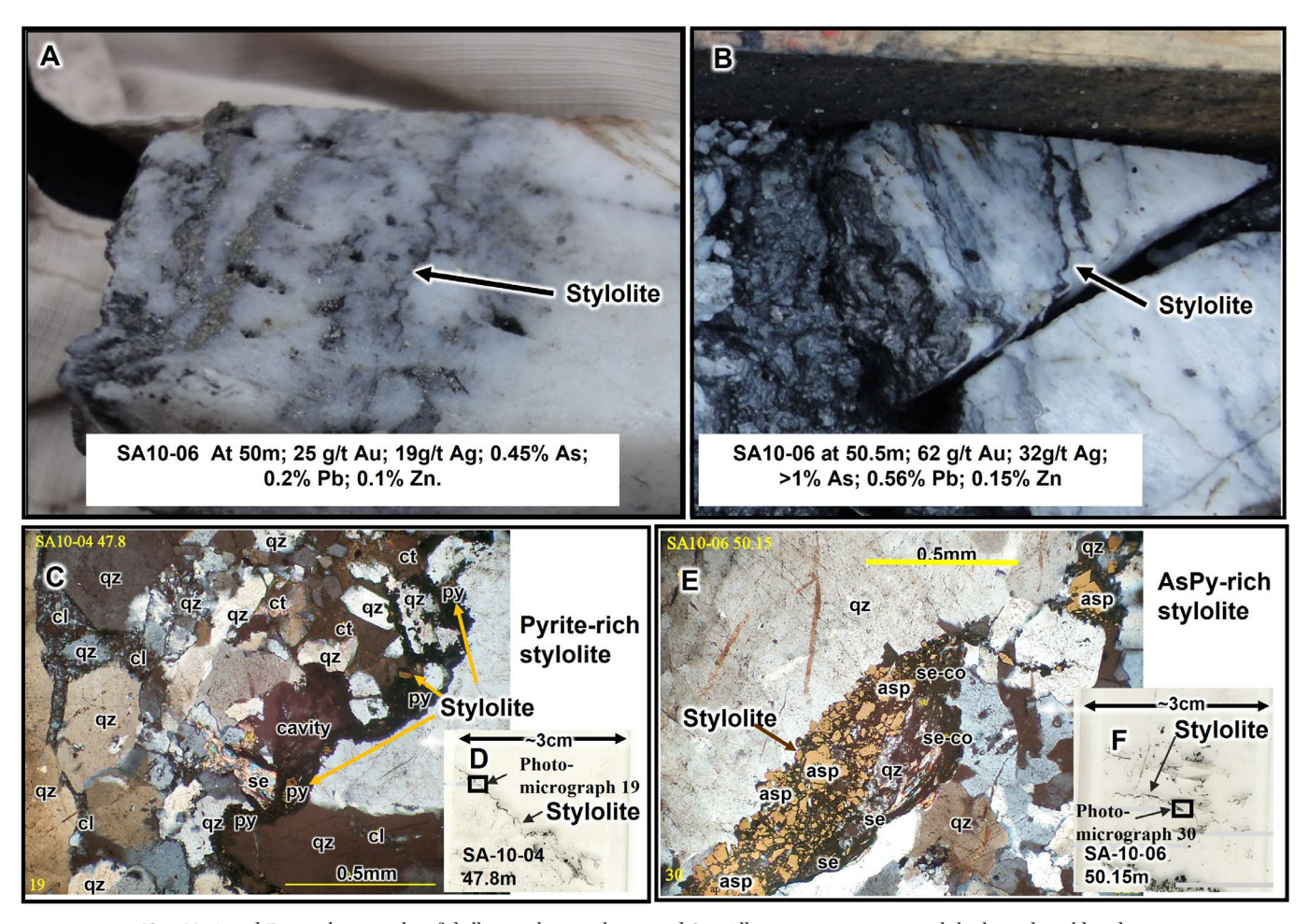


Fig. 11. A and B are photographs of drill core showing laminated San Albino quartz vein set with high-grade gold and stylolites. C. Photomicrograph of stylolite defined by train of granulated pyrite (py) in mineralized quartz vein with interstitial calcite (ct), chlorite (cl), and fine-grained muscovite (sericite) (se). D. Location on thin section of photomicrograph C. E. Photomicrograph of stylolite defined by train of granulated (possibly brecciated?) arsenopyrite (asp) in mineralized quartz vein with slivers of fine-grained muscovite (sericite)-carbonaceous (se-co) country rock. F. Location on thin section of photomicrograph E.

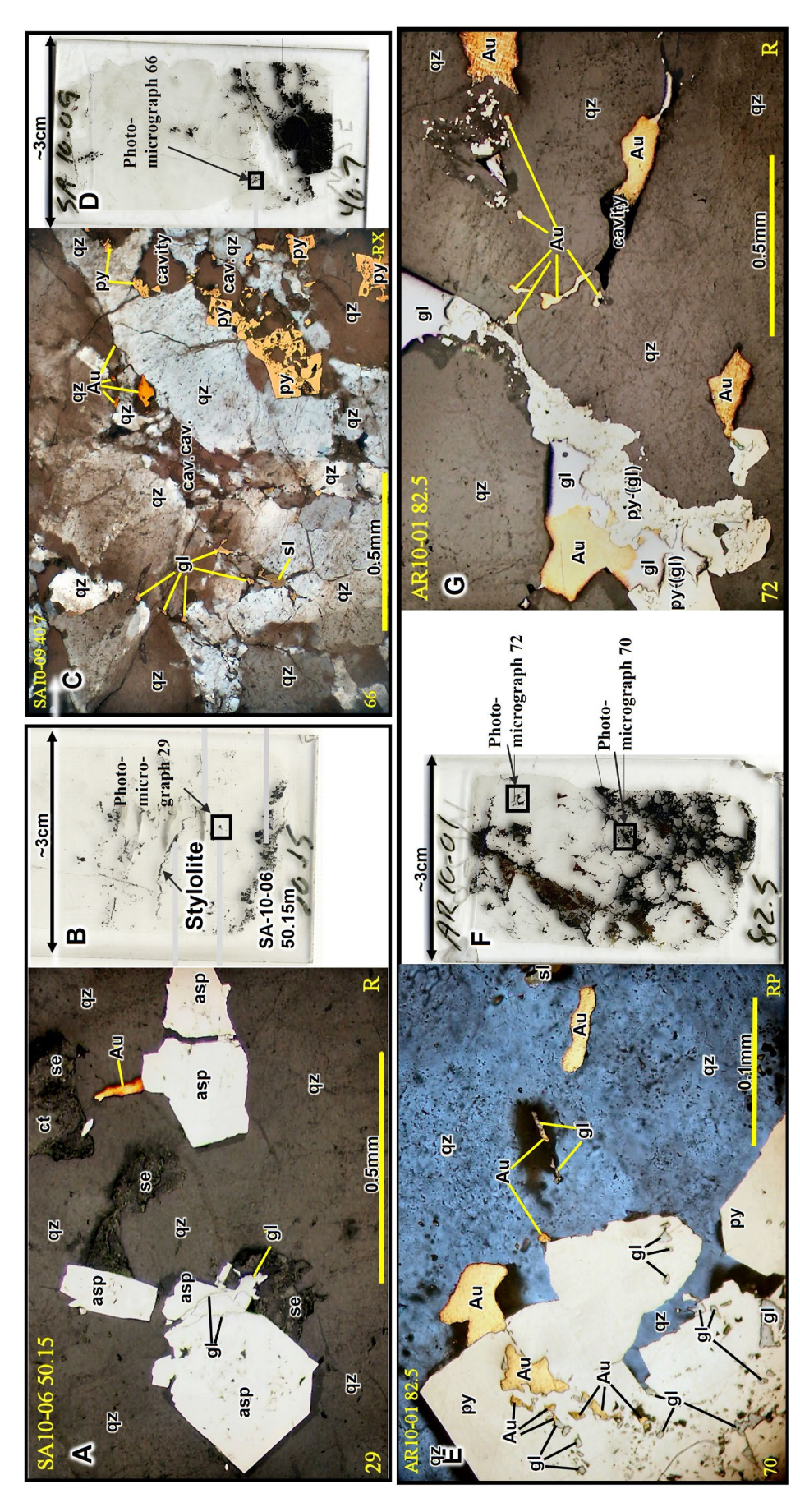
Discussion

Structural evolution of the San Albino deposit

The final stages of accretion of the Mesquito terrane and emplacement of the ~120 to 110 Ma Dipilto batholith (Burianek and Dolnicek, 2011) likely resulted in tectonic burial and metamorphism of the Nueva Segovia schist, but various researchers have suggested alternative causative tectonic events. Rogers (2003) attributed deformation in the Colon fold-and-thrust belt to accretion of the Mesquito (or Siuna) terrane to the Dipilto (or Eastern Chortis) terrane after ~80 Ma. Andjić et al. (2019) more recently attributed the shortening to Late Cretaceous (~90 Ma) formation and docking of the Caribbean large igneous province further to the southeast of the Mesquito terrane. In contrast, a Late Jurassic deformation of the Agua Fria Formation was suggested by Viland et al. (1996). Regardless, the major thrusts of the Colon foldand-thrust belt of Honduras dip to the southeast with vergence toward the northwest (Fig. 2A), while the dominant foliation in the San Albino area dips to the northwest, with

sense of vergence toward the southeast. This local vergence in the opposite direction precludes a simple fold model for the NW-dipping structure that is characteristic of the San Albino deposit and was likely to have controlled mineralization.

We envisage that the NW-dipping rock volume encompassing the Corona del Oro gold belt reflects a back-thrust block that likely developed during progressive Late Jurassic to Late Cretaceous deformation related to accretion of the Mesquito arc. In this interpretation, the Dipilto batholith could have acted as a rheological backstop responsible for promoting a back-thrust wedge during NW-directed thrusting, leading to a favorable structural configuration for San Albino mineralization (Fig. 15). Late stages of the thrusting during rapid exhumation of the subduction-related Dipilto batholith in Albian times (~110–100 Ma) likely initiated the gold-mineralizing event, since such uplift is known to be associated with development of orogenic gold deposition worldwide (Goldfarb and Groves, 2015). While it is possible that mineralization may relate to younger (<80 Ma) deformational events, the mineralized veins at San Albino are displaced by the Mine Creek



pyrite (asp) with galena (gl) and free gold (Åu) in a matrix of quartz (qz) with minor patches of fine-grained muscovite (sericite) (se) and lesser calcite (ct). B. Location on thin section of photomicrograph A. Stylolite shown is described in Figure 11E. C. Quartz vein (qz) with pyrite (py), sphalerite (sl), and galena (gl). Native gold (Au) grains are located on quartz boundaries. cav = cavity. D. Location on thin section slide of photomicrograph C. E. Quartz vein (qz) with pyrite (py) hosting inclusions of galena (gl) and gold (Au), and minor sphalerite (sl). Gold also found along fractures in quartz. F. Location on thin section slide of photomicrograph E (#70) and G (#72). G. Patches of native gold (Au) associated with galena (gl) and pyrite (py) with tiny galena inclusions (py-(gn)). Gold also occurs along cracks in quartz. Fig. 12. Photomicrographs showing gold deportment in quartz veins. A-D from San Albino vein set; E-G from Arras vein set. A. Subhedral to euhedral grains of arseno-

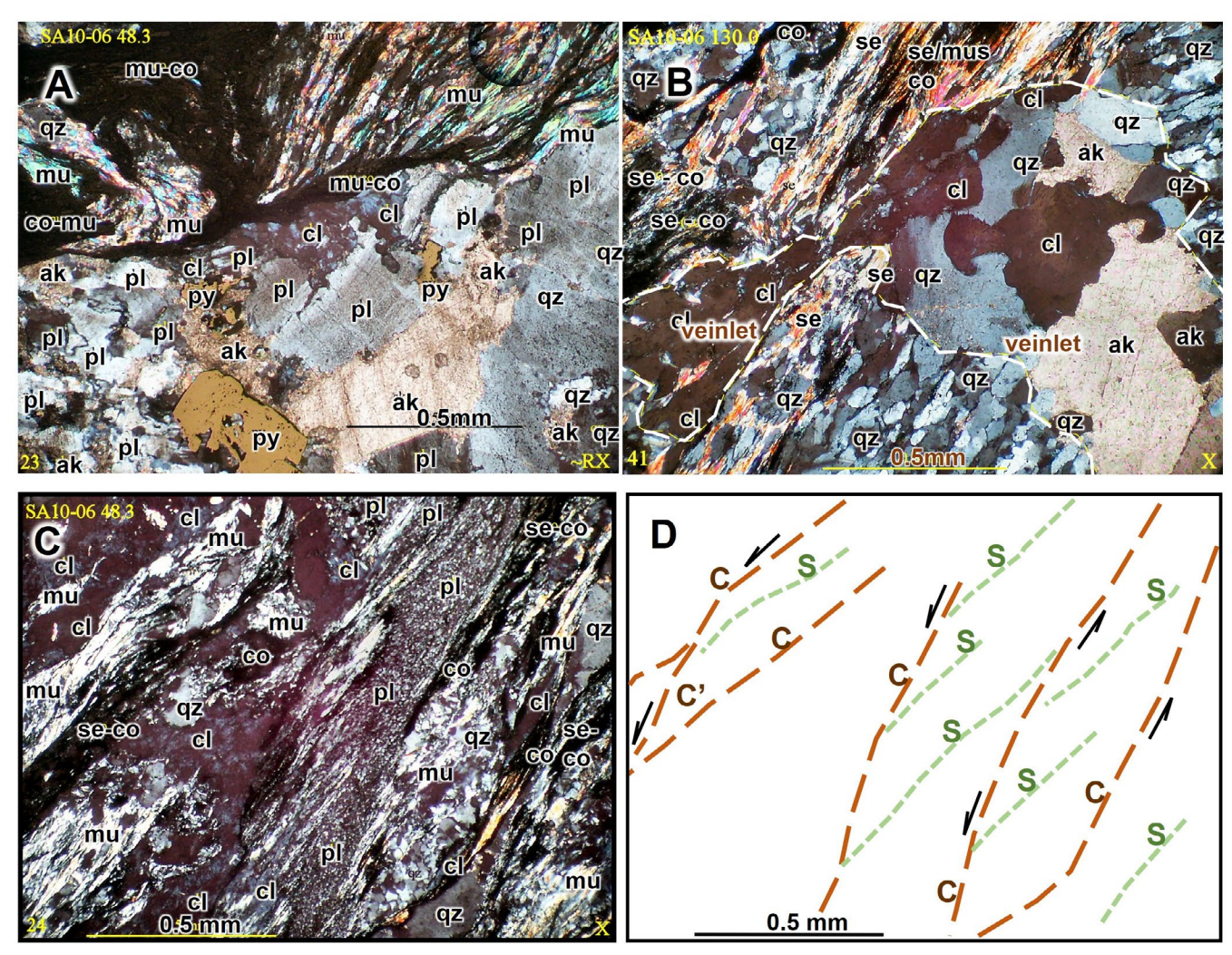


Fig. 13. A-C are photomicrographs showing alteration related to vein mineralization. A and B are from strongly mineralized San Albino vein sets. A. Quartz vein showing coarse-grained ankerite (ak), quartz (qz), plagioclase (pl), and chlorite (cl) cross-cutting foliated schist comprising muscovite (mu), quartz, and carbonaceous material (co). B. Late discontinuous veinlet with much coarser grained, weakly strained minerals up to 0.5 mm wide and comprising chlorite, ankerite, and quartz crosscutting earlier-formed, highly strained quartz vein. C. Strongly deformed quartz-chlorite-ankerite-plagioclase alteration in Naranjo quartz vein set. D. S/C and C' structural interpretation of Naranjo quartz vein set shown in C. se = sericite.

fault (Fig. 6A) and younger normal faults. Thus, we consider that D_2/D_3 shortening occurred in relationship to the initial contractional events. Given additional geochronological constraints, such as dating of crosscutting dikes and metamorphic assemblages, this model could be further refined.

Several lines of evidence support protracted compressional structural development and mineralizing events at San Albino. Development of a younger D_2 -related foliation (S_2) crosscutting the earlier S_1 fabric in fold hinges is the best evidence of the first two distinct deformation episodes. The F_2/F_3 folds associated with and showing the same sense of movement as S/C structures in shear zones are a likely consequence of progressive contractional deformation and widespread brittle-ductile deformation (Fig. 6A). Gold-bearing quartz veins formed in the second and third deformation episodes, with the earlier introduction of quartz during D_2 followed by base metals together with later, dark quartz during D_3 shear-induced brecciation of the earlier white quartz veins (Fig. 10). Not

all gold-bearing quartz veins are brecciated; hence, gold was introduced during both stages of quartz deposition. Indications of more than one gold event are supported by the two geochemically distinct populations of lead/silver/gold and by a distinct inverse relationship between gold and vein thickness above 15 g/t. It is likely that these mineralization episodes are distinct parts of a progressive, heterogeneous brittle-ductile deformation event. Deposition of dark quartz and sulfides in brecciated earlier formed quartz veins reflects implosion breccia sensu Teagle et al. (1990) forming along dilational stepovers along the S₃ fabrics of S/C structures during D₃. A third hydrothermal quartz-rich assemblage comprising weakly deformed quartz-ankerite veins crosscuts strongly recrystallized and sheared veins (Fig. 13). This reflects the last of the vein-forming events and could be either a late D₃ or a temporally distinct D₄ event (Table 3). Development of stylolites within and boudinage of the D₃ mineralized quartz veins leads us to favor a later deformational event(s) (\bar{D}_4 and \bar{D}_5) with

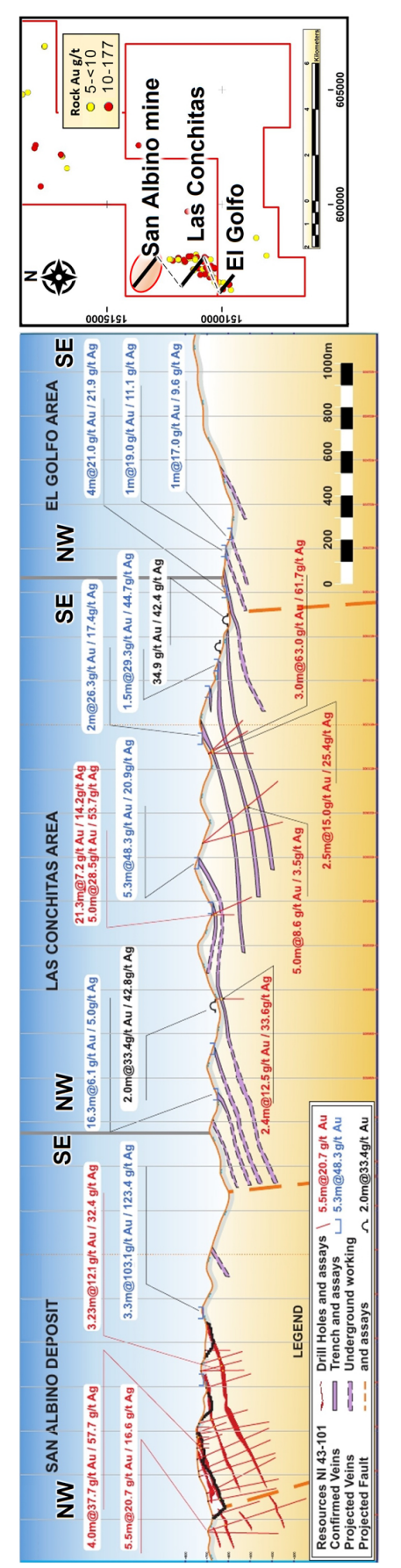


Fig. 14. A fence diagram showing regional stacking of mineralized quartz veins, from the San Albino deposit in the north through Las Conchitas to El Golfo in the south Lipson and Pudar, 2017). Location of fence sections shown in inset map

 D_3 and in part D_4 forming in response to the same transpressional stress regime. Sibson (1994) detailed that flattening perpendicular to the plane of quartz veins is necessary for the development of stylolites. This σ_1 orientation is also consistent with the stress field necessary for necking and boudinaging of quartz veins (Rey, 2016). In other orogenic gold deposits associated with low-angle shear-related quartz veins, such as Nalunaq (Greenland: Gilbertson et al., 2017, figs. 6–14) and Crixas (Goias, Brazil: Ulrich et al., 2021, fig. 7f), extensional veins fill the neck zone between boudins. This supports the presence of a steeply oriented σ_1 stress field as being largely responsible for boudinaging of mineralized quartz veins. At San Albino, regional back thrusting could have caused such steeply oriented σ_1 stresses as the result of a shear-induced stress and thrust-induced loading during D_4 (Fig. 15).

The andesitic dikes and brittle faults, which offset these dikes (Fig. 3B), crosscut all quartz veins and are therefore attributed to a D_5 deformational episode (Table 3). Most dikes strike east-southeast and dip steeply to the south-southwest (Fig. 3C). Hence, it is likely that the dikes developed due to continued ESE-directed stresses responsible for thrusting and that the brittle faults developed later.

The paragenetic sequence described above of vein formation and gold deposition in relation to deformation events is summarized in Figure 16. Mineralized quartz veins developed during D_2 and D_3 , with the majority of gold and sulfide introduction during the D_3 event.

Relative chronology

A middle to late Mesozoic relative chronology of events can be postulated for the local structural evolution and development of the San Albino deposit as follows:

- 1. Middle Jurassic deposition of marginal shallow marine fluvial sediments, minor carbonate, and rhythmically bedded siliciclastic sedimentary rocks of the Neuva Segovia Formation: These were deposited in response to opening of the proto-Caribbean seaway and formed the Dipilto terrane on what was probably attenuated continental crust along the southern margin of the Chortis block (Rogers, 2003).
- 2. Initial, Early Cretaceous collision of the Chortis block (amalgamated Chortis and Dipilto terranes) with the Mesquito island-arc terrane as part of the larger NE-moving Caribbean arc system with consequent subduction from the southeast (Rogers, 2003): Greenschist to local lower amphibolite facies regional metamorphism of the Neuva Segovia Formation overlapped with formation of a NE-trending fold-and-thrust belt. The initial D_1 deformation is best recognized by the regional SE-dipping, NW-vergent foliation in the schistose metapelites in Honduras that formed during the development of the Colon fold-and-thrust belt (Rogers, 2003). Formation of widespread barren and small (<1 m long) quartz veinlets in the San Albino area are products of diagenetic events and/or initiation of prograde metamorphism.
- 3. Late D_1 emplacement of the ~120 to 110 Ma Dipilto batholith immediately northwest of San Albino and at a depth of about 6 km included overprinting by a thermal metamorphic assemblage of cordierite-andalusite-muscovite \pm

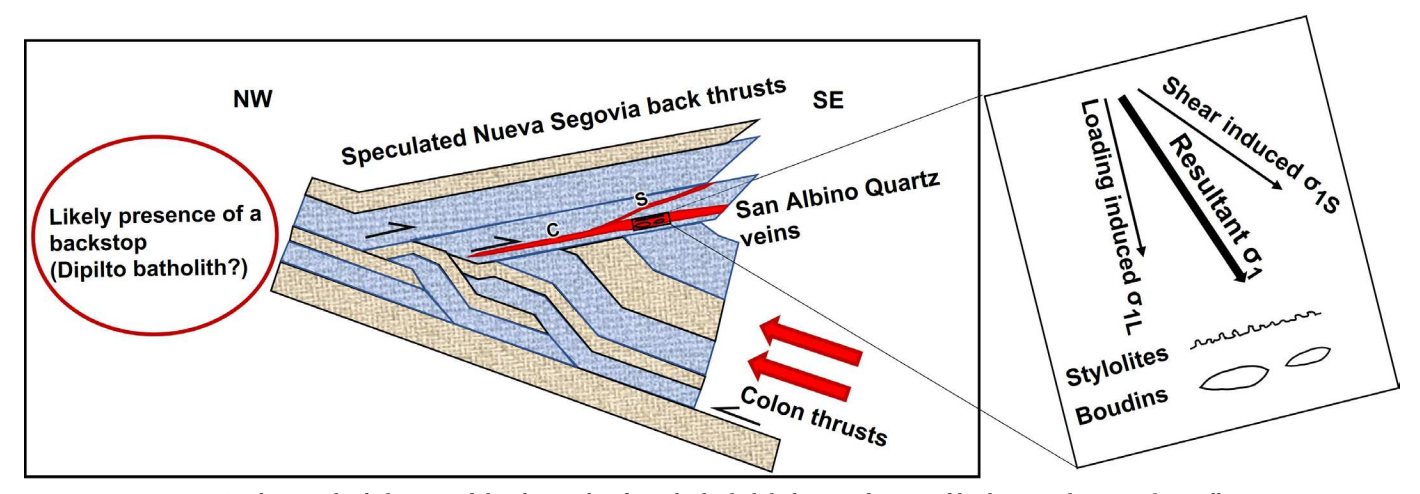


Fig. 15. Schematic back thrust model with postulated Dipilto batholith that acted as a rigid backstop to the west of San Albino deposit, used to explain the local northwest over southeast vergence within the Mako tenements versus the regional southeast over northwest vergence in the Colon fold-and-thrust belt. Quartz veins develop along thrust faults (C surfaces) and along oblique foliations (S surfaces). During the D_4 event of progressive deformation, stylolites developed in mineralized quartz veins, and the veins were boudinaged in response to the resultant σ_1 vector induced by shear and thrust load stresses. Layers are schematic representations of original bedding.

K-feldspar on the regional metamorphic facies in the schist (Burianek and Dolnicek, 2011): The Corona de Oro gold belt, however, is located beyond the limits of the contact aureole, here defined as latest D_1 but distinguished as D_2 by Burianek and Dolnicek (2011).

4. Progressive NW-vergent deformation within the evolving Colon fold-and-thrust belt (Rogers, 2003): This middle Cretaceous (Albian?) deformation included the following: (1) SE-vergent early D2 back thrusting against the Dipilto batholith buttress in the Nueva Segovia area, which resulted in the preexisting D₁ foliation dipping to the northwest (Fig. 15); SE-vergent folding of earlier S_1 foliation led to a new S₂ axial planar foliation (Fig. 4B); (2) formation of D₂ milky fault fill and shear quartz veins with some gold, largely parallel to the main C shear fabric but some also following S fabrics of S/C structures (Fig. 15); these veins locally crosscut foliation at San Albino at a low angle (Fig. 7B); (3) progressive deformation led to D₂/D₃ SE-vergent breaching of folds causing duplication of quartz veins, thickening of ore zones, and deformation of the veins and their alteration zones; (4) main mineralizing event (D₃) with brecciation of the earlier mineralized D₂ quartz veins and simultaneous introduction of gold and base metals along newly formed S structures, forming a matrix to D₂ quartz vein clasts; (5) continued southeast vergence and thrust loading caused intense D₄ flattening resulting in stylolite formation in, and boudinaging of, mineralized quartz veins, in addition to further intense shearing along vein margins; and (6) postmineral D₅ intrusion of andesitic dikes and D₆ brittle faulting overprinted all veins, vein breccias, and dikes.

This deformational history provides a framework in which the San Albino and broader Corona de Oro gold belt can be understood, in order to improve exploration models and relate the style and timing of mineralization to correlative systems in the Americas. Low-angle thrust-related orogenic gold deposits relative to other orogenic gold deposits

Established models for orogenic gold deposit formation have emphasized similarities in structural settings, depth of emplacement, and ore-related fluid sources and ore geochemistry (Goldfarb et al., 2005; Goldfarb and Groves, 2015). While these models provide a robust framework to describe the processes required to form orogenic gold deposits of any age, variations within the generalized models may not adequately describe variations in deposit characteristics. Based on the results of this study, and the comparison with other low-angle, thrust-related orogenic gold deposits described below, we have highlighted this particular low-angle structural style of orogenic gold deposit. These deposits may vary in their distribution of gold grade, including thin, high-grade but discontinuous mineralization within a continuous shear plane, such as San Albino and Nalunaq (this study; Gilbertson et al., 2017); extreme structural dismemberment as at Paracatu (Oliver et al., 2015, 2020); or low-grade disseminated ores associated with brittle-ductile shear veins and extensional veinlets as at Macraes (Allibone et al., 2017, 2018). These variations may lead to significant differences in the mining method and deposit delineation techniques (e.g., open-pit bulk tonnage versus open-pit selective mining versus underground extraction methods).

As with subvertically oriented orogenic gold systems mainly located along high-angle reverse faults, shallowly dipping thrust-related orogenic gold deposits display evidence of multiple fluid flux events. Sibson (1990, 2020) has shown how episodic fault valve behavior can mobilize voluminous pulses of aqueous-carbonic fluid from depth in association with steep reverse faults that are poorly oriented for reactivation and that are close to frictional lockup. In contrast, it is highly unlikely that the multiple fluid events responsible for transporting and depositing gold and quartz at San Albino and similar deposits migrated solely from the downdip extensions

		D_1	D_2	D_3	D_4
	Barren quartz veinlets				
Quartz veins	Milky white quartz veins				
	Dark quartz and major sulfide in veins				
	Au				
Au and sulfides	Py; AsPy				
	Py; AsPy; Ga; Sph; Cp				
Alteration minerals	Qtz; Ser; Chl; Ank; Calc; Plag; (Tm; Rut)		, ——		
	Qtz; Chl; Ank			V	

Fig. 16. San Albino mineral paragenesis in relationship to deformation episodes. Abbreviations: Ank = ankerite, AsPy = arsenopyrite, Calc = calcite, Chl = chlorite, Cp = chalcopyrite, Ga = galena, Plag = plagioclase, Py = pyrite, Qtz = quartz, Rut = rutile, Ser = sericite, Sph = sphalerite, Tm = tourmaline.

of the shallowly dipping thrusts and shear zones controlling these deposits. Tensile overpressures and slow slip may allow large amounts of lateral fluid flow along low-angle structures (Sibson, 2017), but the common sourcing of auriferous fluid migrating from depth via fault-valve action is not obvious. Thus, a fundamental difference exists between the more straightforward way that the unfavorably oriented (sensu Sibson, 1990) steeply dipping orogenic deposits form, relative to the more favorably oriented shallowly dipping thrustrelated styles; perhaps the latter are linked in some way at a downdip location to subvertical faults, but such remains uncertain. Robert and Poulsen (2001) provided a generalized model whereby initiation of low-angle, thrust-related shearing in orogenic gold districts is generally concentrated during D_1 thin-skinned compressional events prior to periods of D_2 thick-skinned shortening and D₃ strike-slip events that tend to be coeval with most gold formation. Likewise, D₃ appears to be the main gold-mineralizing event at San Albino, but as discussed in detail below, the style of deformation remains thinskinned and compressional both earlier than and throughout the mineralizing events. Cawood et al. (2022) have noted that auriferous thrust faults can be reactivated as postgold, low-angle normal faults, such as in the southwestern United States, leading to common deposit misclassification as brittle detachment-type gold deposits. Similar to orogenic gold ores in steep reverse faults, the low-angle, thrust-related orogenic gold deposits are both quartz vein hosted and disseminated within the shear zones associated with the thrusts (Table 1 and references therein). They are commonly developed in metapelitic sequences with a graphitic component. In some examples, such as in overthrusted gneissic sequences (e.g., Pogo, Smith et al., 1999; D. Larimer, writ. commun., 2022), vein walls are lined with graphite, whereas in volcanic rockdominated sequences the veins are located along distinctive rheological heterogeneities that occur between different lithologies (Nalunaq, Gilbertson et al., 2017). Owing to their shallow dips, these deposits lend themselves to open-pit mining more readily than many subvertically oriented orogenic gold deposits.

The San Albino deposit developed along a series of relatively shallowly dipping shear zones typical of many fold-and-thrust belts formed during compressional events. Gold deposits of this structural style are less common in the geologic record

than the above-mentioned subvertical orogenic gold deposits located along and near steeply dipping terrane-bounding faults, such as Obuasi (Fougerouse et al., 2017), Mother Lode (Marsh et al., 2008), and Kalgoorlie-St. Ives (Weinberg et al., 2005). The low-angle, thrust-related orogenic gold deposits can be considered as a somewhat different style of orogenic gold mineralization, and as indicated they may be present either as low-grade bulk tonnage ores or as high-grade compact vein systems, which can be selectively mined. Macraes in South Island, New Zealand (Allibone et al., 2017, 2018), and Paracatu in Brazil (Oliver et al., 2015, 2020) are examples of the former, while examples of the latter include the San Albino deposit (this study), Pogo in Alaska (Smith et al., 1999; Rhys et al., 2003); Crixas in Goias, Brazil (Borges et al., 2021; Ulrich et al., 2021), Nalunag in Greenland (Gilbertson et al., 2017), and Phuoc Son (Manaka, 2014) and Bong Mieu in Vietnam (Stevens and Fulton, 2009) (Fig. 1A; Table 1). All these examples are related to low-angle thrusts that were reactivated during episodes of fluid pressure buildups to form economic gold deposits. Such pressure buildups along structures not normally favorably oriented for such fault valve behavior (Sibson, 2017) could reach lithostatic to supralithostatic conditions if initial hydrothermal events deposited minerals along the thrust to enhance the frictional shear strength. Initial fluid-rock interaction along a shear—perhaps forming hydrothermal feldspars, carbonates, or sulfides—could facilitate large pressure increases, as could any quartz deposition if there were slight temperature decreases along the length of the flow path. A common feature in low-angle, thrust-related orogenic gold deposits is that at least one set of veins occurs parallel or subparallel to the associated low-angle thrust or shear planes, thus creating rheological heterogeneities along which later shear failure and hydrofracturing are more likely to occur. Such later failure with larger pressure fluctuations would cause an abundance of quartz deposition, as silica solubility is extremely sensitive to pressure conditions. However, many of the low-angle gold deposits occur along shear planes defined by incohesive surfaces, most commonly graphite in deformed siliciclastic sediments metamorphosed to greenschist or amphibolite facies. They less commonly occur along zones defined by serpentinite or other relatively ductile units (Table 1). The presence of these less cohesive wall rocks works against large pressure buildups, and thus, in some cases, could

Deformation event	Major manifestation	Quartz vein and mineralization	Associated foliation	Associated folds	Thrusting, shearing, and flattening
D_1	S ₁ foliation Boudinaging of D ₁ quartz veins Intrusion of Dipilto batholith	Boudinaging of barren small quartz veins and veinlets	S ₁ fabric	F_1	Thrusting, shearing, and flattening due to early thrust loading
Progressive deformation © D O	Early mineralizing event S_2 foliation in hinges of F_2 folds S_1 and S_2 drawn into parallelism $(S_{1/2})$ S fabric of S/C structures developed between D_1 quartz vein boudins during D_2 or D_3 SE-vergent thrusting	Milky white laminated mineral- ized quartz veins	S ₂ fabric including S/C structures	$\mathrm{F}_{2/3}$	Development of Nueva Segovia back thrust together with exten- sive shearing
$\frac{\text{Progress}}{\text{D}^3}$	Main mineralizing event S fabric of S/C structures developed between D ₁ quartz vein boudins during D ₂ or D ₃ SE-vergent thrusting	Brecciation of D_2 quartz veins Main mineralizing event Dark laminated quartz vein and sulfide introduction	S ₃ fabric manifest by new S/C structures in quartz veins		Continued back thrust- ing and shearing
D_4	Stylolite development in mineralized quartz veins Boudinaging of mineralized quartz veins				Major flattening due to back thrust load- ing, and continued shearing
D_5 and D_6	Extensional event(s) (relaxation?) with development of subvertical andesitic dike intrusions (D_5) , which are offset by subvertical faults (D_6)				

Table 3. Suggested Framework of Deformational Events at San Albino as Deduced from Relative Structural and Mineralization Relationships

lead to a more disseminated style of gold deposit rather than one characterized by large quartz vein systems.

A variety of mineralized vein styles form during progressive deformation in low-angle, thrust-related orogenic gold deposits. At the San Albino deposit, the gold resource is almost entirely in narrow (m-scale) and laminated (Fig. 7), crack-seal or fault-fill shear-style veins (Figs. 8, 10, 11) with stylolites (Fig. 11) and internal brecciation formed during multiple fluid infiltration events (Fig 10). Progressive deformation localized strain along thrust-related shear zones that parallel the dominant penetrative fabric ($S_{\rm D}$) and along which several stages of mineralized quartz veins developed. The latest of these deformation events include brecciation of the veins with simultaneous precipitation of quartz, sulfides, and additional gold (Table 3; Fig. 16).

In comparison, although some shear-type gold-bearing quartz veins occur at the Macraes deposit, disseminated ores dominate. The crack-seal, laminated, shear-type veins are developed along the thrust plane at the top of the deposit, whereas subvertical extensional stockwork veinlet arrays form in more massive and brittle feldspathic zones of the host schist, and these veins terminate above against the controlling thrust fault (Begbie and Craw, 2006; Allibone et al., 2018), leading Allibone et al. (2018) to conclude that the mineralizing event was simultaneous in both vein systems. Nevertheless, >85%of the gold at Macraes occurs as disseminations in the schist and <15% in the two vein types (Allibone et al., 2018), while in San Albino mineralization is predominately hosted by the veins and immediate (≤0.5 m on either side) contact domains. The disseminated style of gold ore at Macraes may be a result of the enhanced surface area contact between stockwork quartz veinlets and host rock. By contrast, the discrete and extensive sheet-like graphite-rich shear zones along which the

San Albino veins formed likely facilitated more localized strain and hydrothermal fluid flow during progressive deformation, and in addition the carbonaceous schists may have acted as a strong reducing agent, resulting in the formation of more narrow, high-grade ore zones. The lack of extensively developed, laterally continuous auriferous quartz veins with meter-scale thickness is responsible for the relatively low-grade nature of the Macraes deposit, which is mined at 0.82 g/t Au in open pits and 2.59 g/t Au underground (Table 1).

In the Paracatu deposit, three distinct vein types are present, and all are preserved solely as boudins that are mainly parallel to major thrust planes: wider sulfide-rich (up to several percent sulfide) veins averaging 20 mm in thickness by 150 mm in length, narrower sulfide-poor veins (avg 3 mm in thickness by 15 mm in length), and extensional veins (few mm to a few cm in thickness by a few cm to a few tens of cm in length) with coarse-grained sulfides (Oliver et al., 2015). Based on deposit-wide observations, Oliver et al. (2015, 2020) inferred that the veins were originally narrow (tens of cm) even prior to deformation. Although the sedimentary rock fabrics display strong shear characteristics, Oliver et al. (2015) note a strong nonplanar strain flattening, which contributed to boudin development and which may have been induced by shear flow over a sole thrust perturbation (Oliver et al., 2015). Boudinaging has the potential to complicate mining of low-angle, thrust-related orogenic gold deposits because of disaggregation of mineralized domains. In the case of Paracatu, narrow gold zones by themselves are therefore not economic, and bulk mining at a head grade of 0.42 g/t gold takes place over a zone of up to 140 m in thickness (Table 1). In contrast to Paracatu, there is a lack of boudin development at Macraes possibly because of both the dearth of earlier subhorizontal quartz veins and the presence of zones of massive

feldspathic, higher-tensile-strength schist. Thus, while the structural framework of the San Albino, Macraes, and Paracatu deposits is broadly similar, the variations between distribution of gold in sheet-like veins, as disseminations related to veinlet stockworks, or in boudins within each, respectively, are contrasting.

Low-angle quartz veins at the Pogo (Smith et al., 1999), Nalunaq (Gilbertson et al., 2017), Crixas (Borges et al., 2021; Ulrich et al., 2021), Bong Mieu (Stevens and Fulton, 2009; Tran et al., 2014), and Phuc Son (Stevens and Fulton, 2008; Manaka, 2014) deposits are all similar to the meter-scale, laminated crack-seal or fault-fill type of veins at San Albino. Two types of extensional vein sets are also documented from some of these deposits. Pogo and Nalunaq contain extensional vein arrays at high angles to the shallowly dipping veins (Table 1), which at Pogo merge with the fault-fill and laminated crackseal veins and suggest contemporaneous development (Rhys et al., 2003). Similarly at Macraes, the extensional, stockworkstyle quartz veins are also inferred to have developed contemporaneously with the low-angle, thrust-related veins (Allibone et al., 2017, 2018). Both of these indicate broadly contemporaneous brittle-ductile deformation-controlled vein emplacement similar to orogenic gold-bearing vein systems observed along steeply dipping fault systems such as those in Archean greenstone belts (Robert and Poulson, 2001). In contrast, barren or low-grade extensional veins emanating from mineralized quartz vein boudin neck zones at Nalunaq (Gilbertson et al., 2017, figs. 6–14) and Crixas (Ulrich et al., 2021, fig. 7f) suggest development during flattening and boudinage development—an event that postdated main-stage mineralization. Only very local extensional, brittle-type mineralized veins have been recognized at San Albino (Ristorcelli et al., 2020). These observations indicate that a wide variety of structural styles and histories occur within shallow-dipping orogenic gold deposits, such that extensional vein networks may be syngold or postgold at different deposits.

An additional critical factor controlling the higher grade in some low-angle, thrust-related orogenic gold deposits may be the original presence of at least meter-scale, thick laminated quartz veins developed continuously in shear planes preserved at scales of thousands of square meters in plan view. The high-grade (>10 g/t Au) deposits have such features, while the low-grade types are characterized by narrow, discontinuous veins, such as at Paracatu, or stockwork-like quartz veins with disseminated gold, as at Macraes. They may be extremely low grade over enormous thicknesses, such as at Paracatu (0.42 g/t Au over thicknesses of 100–140 m: Sims, 2014; Oliver et al., 2015). The Paracatu example shows that multiple original horizons of thin (tens of cm) but high-grade quartz veins, which were disaggregated by overprinting deformation, are only economic when bulk mined at extremely low grades (<0.5 g/t Au) because of the large volume of intervening waste rock (Oliver et al., 2015, 2020). In contrast, other low-angle deposits show extremely high grades over narrow widths, such as at San Albino (14-21 g/t Au over average vein thicknesses of 1.2 m: Ristorcelli et al., 2020; this study) and at Nalunaq (18.7 g/t Au over 0.5–2 m in thickness: Kaltoft et al., 2000; Gilbertson et al., 2017). High gold grades combined with vein and ore zone continuity at Pogo and Nalunaq have allowed these bodies to be exploited solely from underground. There is a well-defined grade versus thickness continuum across these styles of mineralization from roughly 1 m wide but high-grade (San Albino and Nalunaq) to very thick but low grade (Paracatu) (Fig. 17). A similar relationship, albeit on the scale of a single vein set, has been shown for the San Albino vein above 15 g/t Au (Fig. 9). In summary, the shallowly dipping thrust-related orogenic gold deposits with vein thicknesses in the range of 0.5 to 3 m have the highest grades, while mineralized veins thinner than that are either uneconomic or if stacked can be mined in bulk but at the expense of grade.

Key features of low-angle, thrust-related orogenic gold deposits

Extensive ore footprints along-strike and size potential: The footprints of the total mineralized packages, including exploration targets identified with mineralization, extend much further than just the currently defined economic lodes. The San Albino and related mineralized packages strike for 28 km (this study), Pogo for more than 16 km (J. Rogers, writ. commun., 2022), Phuoc Son more than 7 km (Stevens and Fulton, 2008), Bong Mieu more than 5 km (Stevens and Fulton, 2009), and Crixas more than 5 km (Borges et al., 2021). Some, such as Nalunaq (Gilbertson et al., 2017), are more restricted, extending for only 750 m. The largest of the individual ore lodes have much smaller footprints, e.g., San Albino with 650 \times 300 m (Table 2), Crixas with 3,000 \times 2,000 m (Ulrich et al., 2021), and Pogo with 1,700 \times 500 m (J. Rogers, writ. commun., 2022) (Table 1).

Whereas Paracatu is mined from a single large pit (4,000 m downdip × 3,000 m strike), Macraes was initially developed on a series of small pits along a strike length of ~20 km, which fed a central plant. A few of the individual ore zones grew significantly over time because of further characterization, leading to higher-grade parts being followed underground and culminating in a combined resource >10 Moz Au (Table 1). The San Albino deposit, which crops out and is being successfully mined by open-pit methods, contains sufficient gold grade, thickness (0.5–3 m), and continuity to provide optionality for both surface and underground mining in the future. Implementation of strict grade control to selectively mine these lodes is possible because of the direct association of gold with stacked, continuous, and readily recognizable quartz veins. As happened at Macraes, the regionally extensive Corona de Oro gold belt with its multiple showings of mineralization (Fig. 2B) of similar style to the San Albino deposit has the potential to develop into a much larger global resource with additional exploration.

Ore-shoot downdip/down-plunge dimension exceeding strike dimension: The downdip or down-plunge dimension of individual ore shoots exceeds the ore-shoot strike dimensions for all deposits considered. An early understanding of these geometric features can help to better focus exploration drilling.

Dome or thrust ramp controls on higher-grade gold: At both Paracatu and Macraes, higher gold grades are associated with some form of local steepening of the metasedimentary host-rock package and thus of the low-angle shear zones hosting gold mineralization. This local uplifting may or may not be associated with thick-skinned basement deformation. At

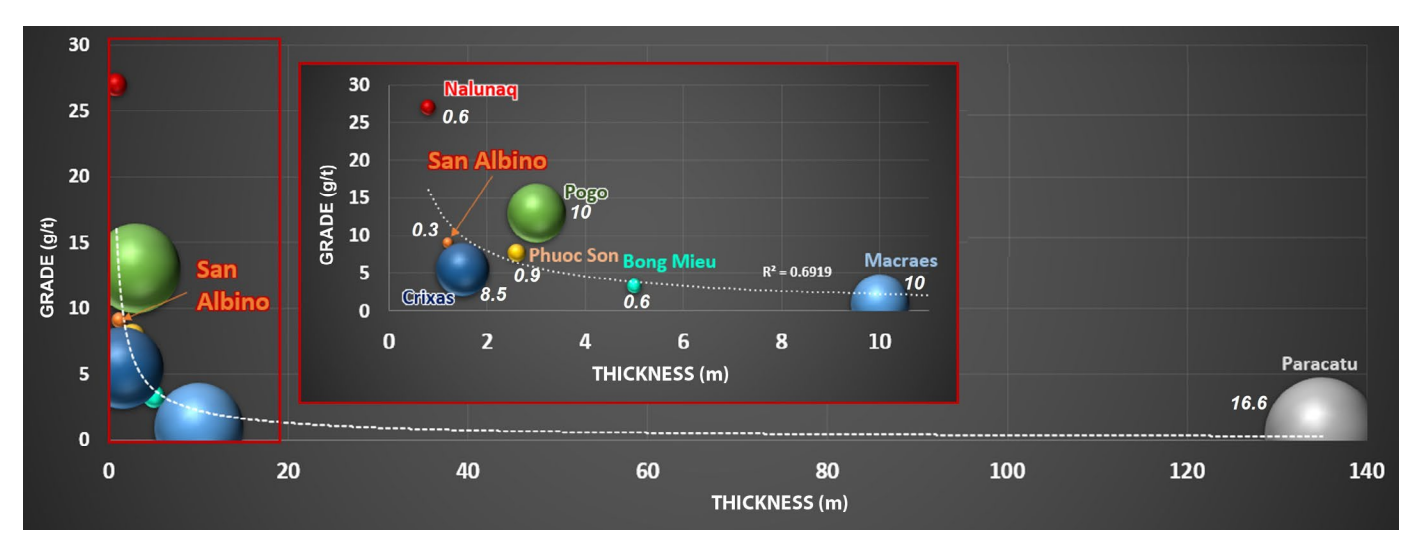


Fig. 17. Gold grade versus average quartz vein thickness (if ≤ 5 m; Fig. 16) or of bulk ore mining width (if > 5 m) in low-angle, thrust-related gold deposits. Central red box is an enlargement of the box on the left-hand side. Bubble size and adjacent numbers reflect known endowment in million ounces of gold, rounded to one decimal place.

Paracatu, Oliver et al. (2015) describe a perturbation in the footwall to the regional thrust or, perhaps, a spatially restricted competency contrast within the stratigraphy, which contributed to the localization of mineralization within a somewhat flattened duplex system branching off the sole thrust. At Macraes, Allibone et al. (2018) describe frontal and lateral ramps of thrusts as areas where higher gold grades are located in minor splays off the hanging-wall shear. The Crixas deposits occur within an anticlinorium centered above the Archean Caiamar Complex comprising tonalite-trondhjemite-granodiorite basement that is depicted as a dome (Ulrich et al., 2021, fig. 13b, c). Bong Mieu is developed within the hinge zone and on both limbs of an anticline (Stevens and Fulton, 2009). Similarly, although shallowly dipping toward the northwest, the San Albino deposit has a dome-like or potentially frontal ramplike shape (Fig. 5), which could reflect some form of deeper footwall perturbation. In combination, these observations suggest that understanding of the broader structural framework, particularly where a steepening of the low-angle structures is notable, is key to defining the mechanisms of deposit formation, vectoring toward the most economic portions of these deposits, and developing more effective mine planning.

Stacked veins: Most of the economic ore deposits discussed have a series of stacked veins, which positively impacts the deposit economics, particularly in the case of open-pit mining (Table 1). This is even true of the low-grade Paracatu deposit where boudins occur discontinuously at different horizons in the metasedimentary package.

The economic potential of these low-angle shear- and thrust-related deposits may easily be overlooked during the exploration stage because of lack of continuity. Although the shear plane horizons along which mineralized quartz veins occur may be recognized, the veins themselves are restricted to specific ore shoots within the planes; the planes may continue along strike and downdip for more than 1 km, but the disjointed nature of the quartz veins means that many drill holes will fail to intercept ore and discourage further exploration. The ubiquitous downdip/down-plunge dimension of

individual ore shoots exceeds the strike dimension, indicating that restricted strike of any one shoot is not necessarily a negative aspect, as seen at San Albino (this study), Crixas (Ulrich et al., 2021, fig. 3), Phuoc Son (Manaka, 2014, figs. 3.2, 3.4), and Bong Mieu (Stevens and Fulton, 2009, fig. 10) where additional shoots are located along strike. Furthermore, structural disruption of mineralized veins due to factors such as boudinaging does not necessarily detract from prospectivity. The geometry of ore shoots may be cryptic, requiring extensive drilling to define grade distribution. Once that has been established, then in many of these deposit types the significant component of largely gravity recoverable free gold (Table 1) may help offset the high initial exploration costs.

Compared with the more steeply dipping types of orogenic gold deposits, these shallowly dipping styles are often overlooked in terms of their economic potential, notwithstanding the far larger footprints they ultimately present after extensive exploration and mining. An understanding of the pinch-and-swell nature of the mineralized portions of prospective shear surfaces and the importance of recognizing pay shoots empowers the explorationist. The ease of open-pit mining at extremely low grades as in the case of Paracatu (Table 1) is also made possible because of the shallow dips.

Conclusions

Orogenic gold deposits are typically recognized as forming during late stages of deformation where near-lithostatic pressures develop along steeply dipping reverse faults that lead to fault-valve behavior in the seismogenic zone (Sibson et al., 1988). This is particularly inherent to active continental margins adjacent to subduction-related batholiths, especially as exhumation of igneous bodies is beginning. The San Albino deposit in northern Nicaragua is a much less common example where orogenic gold deposits formed along low-angle thrusts during thin-skin deformation on the hinterland of such a batholith. Such structures, although typically not severely misoriented for failure, may still undergo fluid cycling where early hydrothermal mineral precipitation can lead to transient

fluid pressure buildups. At San Albino, three major shallowly dipping stacked vein systems were developed along a broad domain of parallel low-angle shears. Progressive shearing and folding along this domain in the middle Cretaceous led to local thickening and brecciation of earlier formed veins, with multiple episodes of metal deposition. The late Albian rapid exhumation of the Dipilto batholith served as a competent buttress for development of the mineralized back thrust wedge.

Despite being a much less common style of orogenic gold deposit, these low-angle ore systems are advantageous for their geometry that facilitates open-pit mining with high strip ratios, either as bulk-tonnage or other more selective above ground or underground targets. Multiple low-angle vein systems along a single narrow shear domain can be perceived as economic targets even if the gold grades are subgram. In many cases, these deposits may undergo post-ore deformation, such as Miocene detachment faulting of Paleocene thrust-related gold deposits in the southwestern United States (e.g., Cawood et al., 2022). Yet even if this leads to a more discontinuous set of orebodies, these relatively horizontal deposits still can be highly economic as bulk tonnage operations.

Acknowledgments

The authors would like to thank Mako Mining Corp. for permission to publish this paper. Special thanks go to site geologists Zoran Pudar, Frank Powell, and Grio Gessner for providing current photographs of pit faces, dike samples, and access to historical data. Stewart Redwood and an anonymous reviewer provided valuable comments, for which they are thanked. In particular, Stewart's incisive editing and suggestions materially helped improve the paper.

REFERENCES

- Allibone, A.H., Jones, P., Moore, J., Craw, D., MacKenzie, D., and Blake-more, H., 2017, Kilometre-scale structural setting of ore shoots in the Frasers gold deposit, Macraes mine, New Zealand: Ore Geology Reviews, v. 89, p. 1107–1121.
- Allibone, A.H. Jones, P., Blakemore, H., Craw, D., MacKenzie, D., and Moore, J., 2018, Structural setting of gold mineralization within the Hyde-Macraes shear zone, southern New Zealand: Economic Geology, v. 113, p. 347–375.
- Andjić, G., Escuder-Viruete, J., Baumgartner-Mora, C., Baumgartner, P.O., Mitchell, S.F., Caron, M., and Caus, E., 2019, Sedimentary record of arccontinent collision along Mesozoic SW North America (Siuna belt, Nicaragua): Tectonics, v. 38, p. 4399–4425.
- AngloGold Ashanti Ltd., 2021, Investing in the future: Mineral resources and ore reserve report, 210 p., www.anglogoldashanti.com/portfolio/americas/serra-grande/.
- Arengi, J.T., and Hodgson, G.V., 2000, Overview of the geology and mineral industry of Nicaragua: International Geology Review, v. 1, p. 45–63.
- Begbie, M.J., and Craw, D., 2006, Geometry and petrography of stockwork vein swarms, Macraes mine, Otago schist, New Zealand: New Zealand Journal of Geology and Geophysics, v. 49, no. 1, p. 63–73.
- Bell, R., Kolb, J., Waight, T.E., Bagas, L., and Thomsen, T., 2017, A Pal-aeoproterozoic multi-stage hydrothermal alteration system at Nalunaq gold deposit, South Greenland: Mineralium Deposita, v. 52, p. 383–404.
- Blandino, B., Martens, U., and Valle, M., 2007, Petrographic and microstructural characterization of greenschist facies rocks in northern Nicaragua: American Geophysical Union, Spring Meeting 2007, San Francisco, California, December 9–14, 2007, Abstracts, U51A-07.
- Bogossian, J., Kemp, A.I.S., and Hagemann, S.G., 2021, Linking gold systems to the crust-mantle evolution of Archean crust in central Brazil: Minerals, v. 11, article 944, p. 1–35.
- Borges, C.C.A., Toledo, C.L.B., Silva, A.M., Kirk, J., Ruiz, J., Chemale, F., Souza, R.G., Santos, B.A., Campos, M.P., Campos, L.M., and Santos, A.M., 2021, Archean to Paleoproterozoic evolution of the Crixas greenstone belt,

- central Brazil: Insights from two contrasting assemblies of metaigneous rocks: Lithos, v. 404–405, p. 1–20.
- Burianek, D., and Dolnicek, Z., 2011, Metamorphic evolution of the contact aureole of the Dipilto batholith, Eastern Chortis terrane, Nicaragua: Journal of Geosciences, v. 56, p. 9–26.
- Carpenter, R.H., 1954, Geology and ore deposits of the Rosario mining district and San Juancito Mountains, Honduras, Central America: Geological Society of America Bulletin, v. 65, p. 23–28.
- Cawood, T.K., Moser, A., Borsook, A., and Rooney, A.D., 2022, New constraints on the timing and character of the Laramide orogeny and associated gold mineralization in SE California, USA: Geological Society of America, GSA Bulletin, v. 134, p. 3220–3241.
- Craw, D., 2005, Macraes gold mine, East Otago, New Zealand: University of Otago, Department of Geology: https://www.otago.ac.nz/geology/research/gold/macraes-gold-mine/.
- De Ronde, C.E.J., Faure, K., Bray, C.J., and Whitford, D.J., 2000, Round Hill shear zone-hosted gold deposit, Macraes Flat, Otago, New Zealand: Evidence of a magmatic ore fluid: Economic Geology, v. 95, p. 1025–1048.
- Edwards, P., Doyle, S., Doelman, P., Cooney, T., and Carr, D., 2020, Macraes gold mine Otago, New Zealand: NI 43-101 Technical Report, 226 p., available at www.sedar.com.
- Elliston, J., 2018, Hydration of silica and its role in the formation of quartz veins—part 1: Substantia, v. 2, no. 2, p. 43–71.
- Fougerouse, D., Micklethwaite, S., Ulrich, S., Miller, J., Godel, B., Adams, D.T., and McCuaig, T.C., 2017, Evidence for two stages of mineralization in West Africa's largest gold deposit: Obuasi, Ghana: Economic Geology, v. 112, p. 3–22.
- Freeborne, S., and Braid, J.A., 2023, Detrital zircon geochronology from the Nueva Segovia schist, Nicaragua: Evidence for the tectonic evolution of the Chortis block: Geological Society, London, Special Publications, v. 531, doi: 10.1144/SP531-2022-185.
- Freitas-Silva, F.H., 1996, Metalogenese do deposito do Morro do Ouro, Paracatu, MG: Unpublished Ph.D. thesis, Brasilia, Brasil, Universidade de Brasilia, 338 p.
- Garcia-Amador, B.I., Alva-Valdivia, L.M., Palacios-Garcia, N.B., and Pompa-Mera, V., 2019, Paleomagnetism and geochronology of the Early Cretaceous Dipilto batholith (NW Nicaragua): Chortis block large rotation with respect to SW North America: Tectonics, v. 39, p. 1–25.
- Garcia-Amador, B.I., Alva-Valdivia, L.M., and Hernandez-Cardona, A., 2021, Syn-tectonic Dipilto batholith (NW Nicaragua) linked to arc-continent collision: High- and room-temperature AMS evidence: Tectonophysics, v. 815, p. 1–17.
- Gazel, E., Flores, K.E., and Carr, M.J., 2021, Architectural and tectonic control on the segmentation of the Central American volcanic arc: Annual Review of Earth and Planetary Sciences, v. 49, p. 495–521.
- Gilbertson, J., Russell, J., Selby, M., and O'Donovan, G., 2017, Technical report on the Nalunaq Gold project, South Greenland: NI 43-101 Technical Report prepared for Amaroq Minerals Ltd. by SRK Consulting, 157 p., www.amaroqminerals.com/projects/nalunaq.
- Goldfarb, R.J., and Groves, D.I., 2015, Orogenic gold: Common or evolving fluid and metal sources through time: Lithos, v. 233, p. 2–26.
- Goldfarb, R.J., Baker, T., Dube, B., Groves, D.I., Hart, C.J., and Gosselin, P., 2005, Distribution, character, and genesis of gold deposits in metamorphic terranes: Economic Geology 100th Anniversary Volume, p. 407–450.
- Graham-Ruzicka, K.L., 2014, Gold-bismuth occurrences in the Kennedy igneous province, North Queensland: Constraints on tectonic, magmatic and hydrothermal processes in intrusion-related gold deposits: Ph.D. thesis, Townsville, Australia, James Cook University, 398 p., http://researchonline.jcu.edu.au/43773/.
- Guillemette, N., and Williams-Jones, A.E., 1993, Genesis of the Sb-W-Au deposits at Ixtahuacan, Guatemala: Evidence from fluid inclusions and stable isotopes: Mineralium Deposita, v. 28, p. 167–180.
- Hanson, W., 2006, Paracatu mine technical report: 159 p., www.sec.gov/ Archives/edgar/data/701818/000118811206000963/tex99_1-9640.txt.
- Instituto Nicaraguense de Estudios Territoriales (INETER), 1995, Mapa geologico minero de la Republica de Nicaragua, Gobierno de Nicaragua: Ministerio de construccion y transporte, scale 1:500,000.
- Jost, H., and Fortes, P.T.F.O., 2001, Gold deposits and occurrences of the Crixas goldfield, central Brazil: Mineralium Deposita, v. 36, p. 358–376.
- Jost, H., Chemale, F., Dussin, I.A., Tassinari, C.C.G., and Martins, R., 2010, A U-Pb zircon Paleoproterozoic age for the metasedimentary host rocks

- and gold mineralization of the Crixas greenstone belt, Goias, central Brazil: Ore Geology Reviews, v. 37, p. 127–139.
- Kaltoft, K., Schlatter, D.M., and Klud, L., 2000, Geology and genesis of Nalunaq Palaeoproterozoic shear zone-hosted gold deposit, South Greenland: Transactions of the Institutions of Mining and Metallurgy, Section B, v. 109, p. 823–833.
- Lipson, R.D., and Pudar, Z., 2017, San Albino: A high grade, free gold, Macraes analogue in Nicaragua: Prospectors and Developers Association of Canada Conference, Toronto, Canada, 2017, Abstracts with Programs, p. 24
- MacKenzie, D.J., and Craw, D., 1993, Structural control of gold-scheelite mineralisation in a major normal fault system, Barewood, eastern Otago, New Zealand: New Zealand Journal of Geology and Geophysics, v. 36, no. 4, p. 437–445.
- Mako Mining Corp., 2023a, Mako mining intersects 33.91 g/t Ggld over 1.7 m estimated true width (ETW) at Las Conchitas Central, 12.73 g/t Au over 4.2 m ETW at Las Conchitas South and multiple high grade silver intercepts up to 3,792.0 g/t silver over 1.0 m across Las Conchitas: Press Release, January 24, 2023, https://makominingcorp.com/news-media/press-releases/index.php?content_id=312.
- Mako Mining Corp., 2023b, Management discussion and analysis for the three months and the year ended December 31, 2022: 20 p., https://makominingcorp.com/investors/financial-reports/.
- Manaka, T., 2014, A study of mineralogical, geochemical and geochronological characteristics and ore genesis in Phuoc Son gold deposit Area, Central Vietnam: Ph.D. thesis, Tasmania, Australia, Centre for Ore Deposit and Earth Sciences (CODES), University of Tasmania, 207 p.
- Manaka, T., Dinh, S.Q., Zaw, K., Meffre, S., Halpin, J., Hai, T.T., Hai, L.V., and Hyng, H.B., 2010, Geology and mineralization of the Phuoc Son gold deposits, central Vietnam: International Association on the Genesis of Ore Deposits (IAGOD) Symposium, Adelaide, Australia, 2010, Proceedings, p. 141–142.
- Marsh, E.E., Goldfarb, R.J., Kunk, M.J., Groves, D.I., Bierlein, F.P., and Creaser, R.A., 2008, New constraints on the timing of gold formation in the Sierra Foothills province, central California: Arizona Geological Society Digest, v. 22, p. 369–388.
- Martini, S.L., 1998, An overview of main auriferous regions of Brazil: Revista Brasileira de Geociencias, v. 28, no. 3, p. 307–314.
- Mattioli, M., Menichetti, M., Renzulli, A., Toscani, L., Salvioli-Mariani, E., Suarez, P., and Murroni, A., 2014, Genesis of the hydrothermal gold deposits in the Canan area, Lepaguare district, Honduras: International Journal of Earth Science, v. 103, p. 901–928.
- McCoy, D., and Olsen, I., 1997, Thermochronology, mineralogy, elemental and microprobe analysis of the Fort Knox, Dolphin and selected Golden Summit deposits: Alaska Miners Association Annual Convention and Trade Fair, Anchorage, Alaska, 1997, Short Course Notes, 15 p.
- Monecke, T., Monecke, J., Reynolds, T.J., Tsuruoka, Ŝ., Bennett, M.M., Skewes, W.B., and Palin, R.M., 2018, Quartz solubility in the H₂O-NaCl system: A framework for understanding vein formation in porphyry copper deposits: Economic Geology, v. 113, p. 1007–1046.
- Mortensen, J.K., Craw, D., MacKenzie, D.J., Gabites, J.E., and Ullrich, T., 2010, Age and origin of orogenic gold mineralization in the Otago schist belt, South Island, New Zealand: Constraints from lead isotope and ⁴⁰Ar/³⁹Ar dating studies: Economic Geology, v. 105, p. 777–793.
- Mortimer, N., Craw, D., MacKenzie, D., Mortensen, J., Ring, U., and Pitcairn, I., 2016, Cretaceous tectonics and gold mineralisation in the Otago schist, New Zealand: Australasian Institute of Mining and Metallurgy (Aus-IMM), Monograph 31, p. 133–140.
- Northern Star Resources Ltd., 2020a, Pogo Q2 operational update: www. listcorp.com/asx/nst/northern-star-resources/news/pogo-q2-operational-update-2286615.html.
- —2020b, Presentation to the gold forum Americas: www.nsrltd. com/investor-and-media/asx-announcements/2020/september/investor-presentation-gold-forum-americas-2020.
- Oliver, N.H.S., Thomson, B., Freitas-Silva, F.H., Holcombe, R.J., Rusk, B., Almeida, B.S., Faure, K., Davidson, G.R., Esper, E.L., Guimarães, P.J., and Dardenne, M.A., 2015, Local and regional mass transfer during thrusting, veining, and boudinage in the genesis of the giant shale-hosted Paracatu gold deposit, Minas Gerais, Brazil: Economic Geology, v. 110, p. 1803–1834.
- Oliver, N.H.S., Thomson, B., Freitas-Silva, F.H., and Holcombe, R.J., 2020, The low-grade, Neoproterozoic, vein-style, carbonaceous phyllite-hosted Paracatu gold deposit, Minas Gerais, Brazil: Society of Economic Geologists, Special Publication 23, p. 101–120.

- Ortega-Gutiérrez, F., Solari, L.A., Ortega-Obregon, C., Elias-Herrera, M., Martens, U., Moran-Ical, S., Chiquin, M., Keppie, J.D., De Leon, R.T., and Schaaf, P., 2007, The Maya-Chortís boundary: A tectonostratigraphic approach: International Geology Review, doi: 10.2747/0020-6814.49.11.996.
- Puritch, E., Sutcliffe, R.H., Burga, D., Yassa, A., Gardner, J., Barry, J., Burga, E., Ray, B., Kuchling, K., Orava, D., Wu, Y., Pearson, J., and Bradfield, A., 2015, Resource estimate and preliminary economic assessment on the San Albino deposit, San Albino-Murra concession, and the El Jicaro concession, Republic of Nicaragua: NI 43-101 and 43 101F1 Technical Report prepared for Golden Reign Resources Ltd. by P&E Mining Consultants Inc., 233 p.
- Ratschbacher, L., Franz, L., Min, M., Bachmann, R., Martens, U., Stanek, K., Stubner, K., and Bock, P., 2009, The North American-Caribbean Plate boundary in Mexico-Guatemala-Honduras: Geological Society, London, Special Publication 328, p. 219–293.
- Redden, R., and Moore, J.G., 2010, Oceanagold technical report for the Macraes project (JORC): 231 p., www.miningdataonline.com/reports/ Macraes_2010_TR.pdf.
- Rey, P.F., 2016, Introduction to structural geology: University of Sydney School of Geosciences, iBooks Series, 87 p., www.geosci.usyd.edu.au/users/ prey/iBooks/Patrice_Textbook.pdf.
- Rĥys, D., DiMarchi, J., Smith, M., Friesen, R., and Rombach, C., 2003, Structural setting, style and timing of vein-hosted gold mineralization at the Pogo deposit, east central Alaska: Mineralium Deposita, v. 38, p. 863–875.
- Ristorcelli, S., Unger, D., and MacFarlane, R., 2020, Technical report and estimate of mineral resources for the San Albino project, Nueva Segovia Nicaragua: NI 43-101 Technical Report for Mako Mining, 115 p., https://makominingcorp.com/_resources/projects/technical-reports/NI43-101-2020-SanAlbino-Final-22.pdf?v=0.027.
- Robert, F., and Boullier, A., 1994, Mesothermal gold-quartz veins and earth-quakes: U.S. Geological Survey, Open File Report 94-228, p. 18–30.
- Robert, F., and Poulsen, K.H., 2001, Vein formation and deformation in greenstone gold deposits: Reviews in Economic Geology, v. 14, p. 111–155.
 Roberts, J.R., and Irving, E.M., 1957, Mineral deposits of Central America: U.S. Geological Survey, Bulletin 1034, 205 p.
- Rogers, D.R., 2003, Jurassic-Recent tectonic and stratigraphic history of the Chortis block of Honduras and Nicaragua (northern Central America): Ph.D. dissertation, Austin, Texas, University of Texas, 265 p.
- Rogers, R.D., Mann, P., and Emmett, P.A., 2007a, Tectonic terranes of the Chortis block based on integration of regional aeromagnetic and geologic data: Geological Society of America, Special Paper 428, p. 65–88.
- Rogers, R.D., Mann, P., Emmett, P.A., and Venable, M.E., 2007b, Colon fold belt of Honduras: Evidence for Late Cretaceous collision, between the continental Chortis block and intra-oceanic Caribbean arc: Geological Society of America, Special Paper 428, p. 129–149.
- Sibson, R.H., 1990, Conditions for fault-valve behavior: Geological Society, London, Special Publication 54, p. 15–28.
- ——1994, Hill fault/fracture meshes as migration conduits for overpressured fluids: U.S. Geological Survey, Open File Report 94-228, p. 224–246, doi: 10.3133/ofr94228.
- ——2017, Tensile overpressure compartments on lowangle thrust faults: Earth, Planets and Space, v. 69, article 113.
- ——2020, Dual-driven fault failure in the lower seismogenic zone: Bulletin of the Seismological Society of America, v. 110, no. 2, p. 1–13.
- Sibson, R.H., Robert, F., and Poulson, K.H., 1988, High-angle reverse faults, fluid-pressure cycling, and mesothermal gold-quartz deposits: Geology, v. 16, p. 551–555.
- Silva-Romo, G., 2008, Guayape-Papalutla fault system: A continuous Cretaceous structure from southern Mexico to the Chortís block? Tectonic implications: Geology, v. 36, p. 75–78.
- Sims, J., 2014, Paracatu project Brazil: NI 43-101 Technical Report for Kinross Gold Corporation, 126 p., https://www.sedar.com/GetFile.do?lan g=EN&docClass=24&issuerNo=00002968&issuerType=03&projectNo=0 2187195&docId=3506540.
- ——2020, Paracatu mine Brazil: NI 43-101 Technical Report for Kinross Gold Corporation, 157 p., https://s2.q4cdn.com/496390694/files/doc_downloads/technical_reports/2020/04/Kinross-Paracatu-NI43-101-Mar-10-2020.pdf.
- Smith, M., Thompson, J.F.H., Bressler, J., Layer, P., Mortensen, J.K., Abe, I., and Takaoka, H., 1999, Geology of the Liese zone, Pogo property, east-central Alaska: SEG Newsletter, no. 38, p. 1–21.
- Squires, B., Frieman, B.M., Monecke, T., and Powell, F., 2022, Unraveling the structural history of orogenic gold deposits in the Corona de Oro gold belt, northwestern Nicaragua: Geological Society of America Meeting,

Denver, Colorado, 2022, Abstracts with Programs, 15 p., doi: 10.1130/ abs/2022AM-383511.

- Stevens, M.R., and Fulton, G.W., 2008, Technical report on feasibility studies for the Phuoc Son gold project in Quang Nam province, Vietnam: NI 43-101 Technical Report for Olympic Pacific Minerals Inc., 324 p., https://www.sec.gov/Archives/edgar/data/1164099/000119907308000300/ex99_1. htm.
- ——2009, Updated technical review of Bong Mieu gold project in Quang Nam province, Vietnam: NI 43-101 Technical Report for Olympic Pacific Minerals Inc., 198 p., https://www.sec.gov/Archives/edgar/data/1164099/000119907309000382/ex99_1.htm.
- Teagle, D.A.H., Norris, R.J., and Craw, D., 1990, Structural controls on gold-bearing quartz mineralization in a duplex thrust system, Hyde-Macraes shear zone, Otago schist, New Zealand: Economic Geology, v. 85, p. 1711–1719.
- Thompson, W.D., 2020, Geochemical, spatial, and temporal relationships of the intrusives and meta-intrusives of the Pogo deposit, Eastern Interior, AK: M.Sc. thesis, Fairbanks, Alaska, USA, University of Alaska, Fairbanks, 138 p.
- Tran, T.T., Zaw, K., Halpin, J.A., Manaka, T., Meffre, S., Lai, C., Lee, Y., Le, H.V., and Dinh, S., 2014, The Tam Ky-Phuoc Son shear zone in central Vietnam: Tectonic and metallogenic implications: Gondwana Research, v. 26. p. 144–164.
- Ulrich, S., Hageman, S., Charão, J.M., Figueiredo, F.L.A.R., Ramires, J.E.F., Frantz, J.C., and Petersen, K., 2021, The orogenic Crixas gold deposit, Goias, Brazil: A review and new constraints on the structural control of ore bodies: Minerals, v. 11, p. 1–27.
- Venable, M.E., 1994, A geologic, tectonic and metallogenic evaluation of the Siuna terrane: Ph.D. dissertation, Tucson, Arizona, USA, University of Arizona, 154 p.
- Viland, J., Henry, B., Calix, R., and Diaz, C., 1996, Late Jurassic deformation in Honduras: Proposals for a revised regional stratigraphy: Journal of South American Earth Sciences, v. 9, p. 153–160.

- Wang, B., Gough, L.P., Wanty, R.B., Crock, J.G., Lee, G.K., Day, W.C., and Vohden, J., 2007, Landscape geochemistry near mineralized areas of eastern Alaska: U.S. Geological Survey, Scientific Investigations 2007-5289, p. H1-H8
- Weinberg, R.F., Van der Borgh, P., Bateman, R.J., and Groves, D.I., 2005, Kinematic history of the Boulder-Lefroy shear zone system and controls on associated gold mineralization, Yilgarn craton, Western Australia: Economic Geology, v. 100, p. 1407–1426.

Rael Lipson is a consulting exploration geologist, director of Mako Mining Corp., which operates the San Albino mine, and cofounder and director of Annamite Resources Holdings Pte. Ltd., which is exploring in Laos. His earlier corporate career of 42 years culminated in the position of chief exploration geologist with Gold Fields Ltd. From a Denver



base, he helped guide area selection, assessed projects globally, and assisted in corporate exploration projects, drawing from earlier base metal, paleoplacer, and orogenic gold experience. He holds a Ph.D. degree (geochemistry) from the University of Cape Town and an M.Sc. degree (geology) from the University of the Witwatersrand.